2302–2318 *Nucleic Acids Research, 2022, Vol. 50, No. 4* *Published online 8 February 2022*
https://doi.org/10.1093/nar/gkac062

Epitranscriptomic regulation of HIV-1 full-length RNA packaging

Camila Pereira-Montecinos[1,2], Daniela Toro-Ascuy[1,2,3], Catarina Ananías-Sáez[1,2], Aracelly Gaete-Argel[1,2], Cecilia Rojas-Fuentes[1,2], Sebastián Riquelme-Barrios[1,2], Bárbara Rojas-Araya[1,2], Francisco García-de-Gracia[1,2], Paulina Aguilera-Cortés[1,2], Jonás Chnaiderman[1], Mónica L. Acevedo[1,3], Fernando Valiente-Echeverría[1,2,3] and Ricardo Soto-Rifo[1,2,3,*]

[1]Laboratory of Molecular and Cellular Virology, Virology Program, Institute of Biomedical Sciences, Faculty of Medicine, Universidad de Chile, Santiago, Chile, [2]HIV/AIDS Workgroup (CHAIR), Faculty of Medicine, Universidad de Chile, Santiago, Chile and [3]Millennium Institute on Immunology and Immunotherapy, Santiago, Chile

Received March 13, 2021; Revised January 17, 2022; Editorial Decision January 18, 2022; Accepted January 25, 2022

ABSTRACT

During retroviral replication, the full-length RNA serves both as mRNA and genomic RNA. However, the mechanisms by which the HIV-1 Gag protein selects the two RNA molecules that will be packaged into nascent virions remain poorly understood. Here, we demonstrate that deposition of N^6-methyladenosine (m^{6}A) regulates full-length RNA packaging. While m^{6}A deposition by METTL3/METTL14 onto the full-length RNA was associated with increased Gag synthesis and reduced packaging, FTO-mediated demethylation promoted the incorporation of the full-length RNA into viral particles. Interestingly, HIV-1 Gag associates with the RNA demethylase FTO in the nucleus and contributes to full-length RNA demethylation. We further identified two highly conserved adenosines within the 5′-UTR that have a crucial functional role in m^{6}A methylation and packaging of the full-length RNA. Together, our data propose a novel epitranscriptomic mechanism allowing the selection of the HIV-1 full-length RNA molecules that will be used as viral genomes.

INTRODUCTION

Retroviral full-length RNA (FL-RNA) plays two key functions in the cytoplasm of infected cells. First, it is used as the mRNA template for the synthesis of Gag and Gag-Pol precursors and, second, it serves as the genomic RNA (gRNA) packaged into newly produced viral particles (1–3). In contrast to the simple retrovirus murine leukemia virus (MLV), which was shown to segregate its FL-RNA into two functionally different populations serving as template for translation (mRNA) or packaging (gRNA), the FL-RNA from HIV-1 was proposed to exist as a single population acting indistinctly as mRNA or gRNA (4–6). More recent evidence showed that despite this property, a given FL-RNA molecule can accomplish only one function at a time (7). However, and despite several years of efforts, there is still an important gap in our knowledge regarding the molecular mechanisms behind the selection of the FL-RNA molecules that will be incorporated into assembling viral particles.

During the late steps of the replication cycle, the nucleocapsid (NC) domain of the Gag protein recognizes *cis*-acting RNA elements present mainly at the 5′-untranslated region (5′-UTR) and drives the selective incorporation of two copies of the gRNA into assembling viral particles. Indeed, there is accumulating evidence showing that dimerization and packaging of the HIV-1 FL-RNA are two tightly interconnected processes dependent on the Gag protein (8–11). Structural and mutational analyses proposed that a conformational switch within the 5′-UTR regulates the transition from translation to dimerization and packaging *in vitro* (12–15). In such models, the 5′-UTR alternates in conformations that occlude the dimerization initiation signal (DIS) or the Gag start codon ('U5/AUG' conformation) thus, favoring translation or dimerization and packaging, respectively (3,16). However, chemical probing performed in cells and viral particles showed that it is difficult to distinguish between these two different proposed structural models (17–19). As such, chemical probing *in cellulo* and *in virio* is consistent with a dimerization prone conformation of the 5′-UTR featuring the U5/AUG pairing and leaving DIS the possibility to form a 'kissing' dimer (17,19,20). Moreover, the packaging prone structure

*To whom correspondence should be addressed. Tel: +56 2 2978 68 69; Email: rsotorifo@uchile.cl
Present address: Daniela Toro-Ascuy, Instituto de Ciencias Biomédicas, Facultad de Ciencias de la Salud, Universidad Autónoma de Chile, Santiago, Chile.

© The Author(s) 2022. Published by Oxford University Press on behalf of Nucleic Acids Research.
This is an Open Access article distributed under the terms of the Creative Commons Attribution-NonCommercial License (http://creativecommons.org/licenses/by-nc/4.0/), which permits non-commercial re-use, distribution, and reproduction in any medium, provided the original work is properly cited. For commercial re-use, please contact journals.permissions@oup.com

Downloaded from https://academic.oup.com/nar/article/50/4/2302/6524254 by guest on 11 April 2024

does not interfere with FL-RNA translation suggesting that other factors are involved in the regulation of the cytoplasmic sorting of the HIV-1 FL-RNA (21,22).

It was recently reported that the HIV-1 FL-RNA contains N^6-methyladenosine (m^6A) residues located at the 5′- and the 3′-UTR as well as at internal positions such as the Rev response element (RRE) (23–25). Methylation of adenosines at the RRE and the 3′-UTR was shown to promote Gag synthesis by favoring nuclear export and/or the intracellular accumulation of viral transcripts at late stages of the replication cycle (23–26). However, it was also reported that the presence of m^6A could also induce the degradation of the incoming viral genome early during infection (25,26). These controversial data prompted us to study whether m^6A could serve as a mark that defines the functions of the HIV-1 FL-RNA as template for translation or packaging during viral replication.

Here, we show that methylation of the FL-RNA by the METTL3/METTL14 complex inhibits packaging. MeRIP-seq analysis revealed that the FL-RNA present in purified viral particles lacks m^6A at the 5′-UTR suggesting the existence of two populations that differ in their m^6A patterns. We further identify two highly conserved adenosines, A_{198} and A_{242}, as key residues for the regulation of FL-RNA packaging. We also observed that the FL-RNA is a substrate for the RNA demethylase FTO, which together with Gag drives RNA demethylation to promote packaging. As such, the pharmacological targeting of FTO activity resulted in impaired FL-RNA metabolism and a strong inhibition of packaging. Together, our data reveal a novel mechanism by which Gag selects the RNA molecules that will be used for packaging, which is regulated by FTO-mediated demethylation of the FL-RNA.

MATERIALS AND METHODS

DNA constructs

The pNL4.3ΔEnv provirus (from here named as pNL4.3) was previously described (27). The pNL4.3-Δ198, pNL4.3-Δ242 and pNL4.3-Δ198/Δ242 mutant proviruses were obtained by site-directed mutagenesis using pNL4.3 as a template and the primers showed in Supplementary Table 3. pCMV-VSVg was previously described (28). The pCDNA-Flag-METTL3 and pCDNA-Flag-METTL14 were a gift from Dr Chuan He (Addgene plasmid #53739 and #53740, respectively) and were previously described (29). pCDNA-d2EGFP was previously described (27). The pCDNA-3XFlag-FTO and pEGFP-ALKBH5 were a gift from Dr Yun-Gui Yang (Beijing Institute of Genomics, Chinese Academy of Sciences) and were previously described (30,31). pCDNA-3XFlag-d2EGFP was generated by replacing the FTO cDNA from pCDNA-3XFlag-FTO by the d2EGFP ORF. The pNL4.3-GagStop vector was previously described (32). The pCDNA-Gag vector was previously described (33). The pNL4.3-EGFP-Puro vector was previously described (34). The pBSK-Gag/Pol used for the generation of biotinylated probes was previously described (32).

Cell culture, DNA transfection and viral particle purification

HEK293T and HeLa cells were maintained in DMEM (Life Technologies) supplemented with 10% FBS (Hyclone) and antibiotics (Hyclone) at 37ºC and 5% CO_2 atmosphere. SupT1 cells were maintained in RPMI (Life technologies) supplemented with 10% FBS (Hyclone) and antibiotics (Hyclone) at 37ºC and 5% CO_2 atmosphere. Cells growing in 6-well plates (2.5×10^5 cells/well) were transfected with 0,6 μg of proviral vector together with 0,6 μg of pCMV-VSVg and 2 μg of METTL3 and METTL14 or 4 μg of FTO/ALKBH5 coding plasmids using a ratio μg DNA/μl PEI of 1/15 (linear PEI ∼25 000 Da; Polyscience) as described previously (27). For experiments involving the FTO inhibitor, the culture medium was replaced by medium containing dimethyl sulfoxide (DMSO) as a control or 80 μM of an ethyl ester form of meclofenamic acid diluted in DMSO (MA2) prior DNA transfection. For viral particle concentration, the supernatant was collected and filtered by passing through a 0.22 μm filter and then either ultracentrifugated at 25 000 rpm for 2 h at 4ºC in a 20% sucrose cushion (prepared previously and stored at 4ºC) or concentrated with the Lenti-X™ Concentrator (Takara). Purified viral particles were resuspended in 100 μl of PBS and stored in aliquots at −80ºC to then perform anti-CAp24 ELISA (HIV-1) or western blot (MLV) or RNA extraction. Cells were also collected to perform western blot and RNA extraction as described below.

MeRIP-seq

Poly(A) RNA was purified from 100 μg of total RNA extracted from HEK293T cells previously transfected with 5 μg of pNL4.3-EGFP-Puro and 5 μg of pCMV-VSVg. Briefly, total RNA in 500 μl of water was incubated at 65º C for 10 min and incubated with 3 μl of oligo dT-Biotin (dT-B; IDT Technologies) (50 pmol/μl) and 13 μl of SSC Buffer 20× (Santa Cruz Biotechnologies) and allowed to cool at room temperature. 600 μg of Dynabeads™ Streptavidin (60 μl; Thermo Fisher) were washed three times with Buffer SSC 0.5X and resuspended in 100 μl of Buffer SSC 0.5×. Then, the RNA/oligo dT-B mix was incubated with the streptavidin beads at room temperature for 10 min in head-over-tail rotation. RNA-beads were washed four times with 300 μl Buffer SSC 0.1× and bound RNA was eluted twice with 100 μl of water. The RNA was precipitated with 10 mM $MgCl_2$, 20 μg glycogen (Thermo Fisher) and 2.5 volume of ETOH 100% overnight at −20ºC and then washed with ETOH 70%. Poly(A) RNA as well as RNA obtained from concentrated viral particles were fragmented using Fragmentation Reagent (Thermo Fisher). For this, 2 μg of RNA in 9 μl of water was incubated with 1 μl of Fragmentation Buffer 10× for 15 min at 70ºC, then 1 μl of Stop solution was added and incubated on ice. The RNA fragmented was precipitated overnight as described above. Fragmented RNA diluted in 380 μl was heated at 70ºC for 5 min, placed on ice for 3 min. The denatured RNA was mixed with 1 μl of rRNasin® (Promega), 5 μl VRC, 100 μl of IP Buffer 5X (50 mM Tris–HCl pH 7.4, 750 mM NaCl and 0.5% NP-40) and 5 μl of an anti-m^6A antibody (0.5 mg/ml; Synaptic System #202003) and incubated for 2 h at 4ºC with

Downloaded from https://academic.oup.com/nar/article/50/4/2302/6524254 by guest on 11 April 2024

head-over-tail rotation. At the same time, 600 μg of Dynabeads™ Protein A magnetic beads (20 μl; Thermo Fisher) were washed in 1 ml of IP Buffer 1× with 1 μl of VRC and were incubated with 500 μl of Buffer IP 1× with 0.5 mg/ml of BSA for 2 h at 4ºC with head-over-tail rotation. Then, beads were washed with 500 μl of IP Buffer 1× and added to the RNA/anti-m^{6}A antibody mix. The RNA-beads mix was incubated for 2 h at 4ºC in head-over-tail rotation. After incubation, the RNA-beads mix was washed twice with 500 μl IP Buffer 1×. Bound RNA was eluted with 100 μl of Elution Buffer (5 mM Tris–HCl pH 7.5; 1 mM EDTA and 0.05% SDS) and 1 μl of Proteinase K (New England BioLabs) and incubated for 1.5 h at 50ºC. RNA was extracted from supernatant using TRIzol (Thermo Fisher). The RNA recovered was precipitated with 10 mM $MgCl_2$, 20 μg glycogen (Thermo Fisher) and 2.5 volumes of ETOH 100% overnight at −20ºC and then washed with ETOH 70%. Equal amounts of RNA from input and immunoprecipitation were used for RT-qPCR. cDNA libraries preparation and RNAseq was performed as a service from Genoma Mayor at Universidad Mayor, Chile. All the samples were sequenced in an Illumina HiSeq2000 platform with paired-end 100 bp read length. Read quality was evaluated with *Fastqc* and the *Burrows-Wheeler Alignment Tool (BWA - Mem)* was used for mapping reads to the HIV-1 genome with default parameters (Supplementary Table 1).

Data were plotted as FPKM and correspond to the reads from the MeRIP-seq data normalized by the input data. Peak calling analysis was performed using MACS2 version 2.1.1.20160309 (35). The *P* value for each nucleotide in the FL-RNA was calculated and then the Benjamini-Hochberg method was used to correct multiple comparisons and convert *P* value into *q* value or a minimal FDR to find significance for each peak. The *q* value used was 0.05 corresponding to an FDR of 95%. A detailed summary of the bioinformatic analyses can be found at the Supplementary materials available at NAR online.

RNA extraction and RT-qPCR

RNA extraction and RT-qPCR was performed essentially as recently described (32). Briefly, cells were washed and recovered with PBS-EDTA 10 mM. Cells in PBS were centrifuged at 5000 rpm for 5 min at 4ºC cell pellets were resuspended in 200 μl of PBS. Cells or purified viral particles were used to perform RNA extraction by adding 1 ml of TRIzol™ (Thermo Fisher) and 200 μl of chloroform (Merck). The mix was vortexed vigorously and centrifuged at 10 000 rpm for 5 min at 4ºC. The aqueous phase was recovered, incubated for 5 min with an equal volume of 2-propanol (Merck), and centrifuged at 12 000 rpm for 20 min at 4ºC. The RNA pellet was washed with ETOH 70% (Merck) and resuspended in ultrapure water. RNAs obtained were treated with TURBO DNA-free kit (Thermo Fisher) for 30 min at 37ºC as indicated by the manufacturer. RNA from viral particles were obtained as above using 20 μl of concentrated particles diluted in 180 μl of PBS 1×. RNAs were reverse-transcribed using the High Capacity RNA-to-cDNA Master Mix (Thermo Fisher) or the KAPA SYBR® FAST One-Step (Sigma-Aldrich) as indicated by the manufacturer. For intracellular RNAs, 300 ng (High Capacity RNA-to-cDNA Master Mix) or 50 ng (KAPA SYBR® FAST One-Step) were used to perform cDNA synthesis or RT-qPCR in all tested conditions. For RNA obtained from viral particles, we used 300 ng of RNA (High Capacity RNA-to-cDNA Master Mix) or 50 ng (KAPA SYBR® FAST One-Step) from the corresponding control condition as a reference and the amount of RNA from the tested condition was adjusted according to the CAp24 levels obtained by ELISA to quantify FL-RNA from CAp24 equivalents. All reverse transcription reactions included a no-RT control, adding RNA but not the RT enzyme to corroborate efficient DNAse treatment. For qPCR using cDNAs obtained with the High Capacity RNA-to-cDNA Master Mix, a 25 μl reaction mix was prepared with 5 μl of template cDNAs (previously diluted to 1/10), 12.5 μl of Brilliant II SYBR® Green QPCR Master Mix (Agilent Technologies), 0.4 μl of sense and antisense primers (stored in a mix a 10 mM) and 7.1 μl of water. The reaction mix was subjected to amplification using the AriaMx Real-Time PCR System (Agilent Technologies). For intracellular RNAs, the GAPDH housekeeping gene was amplified in parallel to serve as a control reference. In addition to the no-RT control, a no-cDNA negative control using water and the qPCR mix was included in every qPCR experiment. In the case of intracellular RNA, relative copy numbers of HIV-1 full-length RNA were normalized to GAPDH using $x^{-\Delta Ct}$ (where x corresponds to the experimentally calculated amplification efficiency of each primer couple). All our qPCR reactions are in the linear range of the assay. Primers used for RT-qPCR are described in Supplementary Table 4. Relative copy numbers were expressed as the percentage of the respective control condition.

Western blot

Extracts from transfected HEK293T cells were prepared by resuspending cell pellets in lysis buffer (150 mM NaCl, 1% NP-40 and 50 mM Tris–HCl pH 8.0). 30 μg of total protein from cell lysates were subjected to 10% SDS-PAGE and transferred to an Amersham Hybond-P 0.45 PVDF membrane (GE Healthcare) for 2 h, 0.4 A at 4ºC. Membranes were blocked with Blotting-Grade Blocker (Bio-Rad) for 1 h at room temperature and were incubated with the corresponding primary antibody; a mouse HIV-1 p24 monoclonal antibody diluted to 1/1000 (NIH AIDS Reagents Program, #3537), a rabbit anti-Flag antibody (Sigma-Aldrich, #637303) diluted to 1/1000, a mouse anti-GAPDH diluted 1/5000 (Santa Cruz Biotechnologies, #sc-51905) or a mouse anti-Actin diluted 1/5000 (Santa Cruz Biotechnologies, #sc-47778). Upon incubation with the corresponding HRP-conjugated secondary antibody (Jackson ImmunoResearch) diluted to 1/5000, membranes were analyzed with the Pierce® ECL Substrate or the SuperSignal™ West Femto (Thermo Scientific) using a MiniHD9 Western Blot Imaging System scanner (Uvitec Cambridge).

ELISA

The anti-CAp24 ELISA (R&D SYSTEMS, catalog number DHP240B) was performed as indicated by the manufacturer. Briefly, viral particles concentrated by ultracentrifugation and resuspended in PBS were mixed with the

Downloaded from https://academic.oup.com/nar/article/50/4/2302/6524254 by guest on 11 April 2024

Calibrator Diluent RD5-26 (diluted 1/4). Then, 100 μl of the Assay Diluent RD1-124 were added in the well coated with a monoclonal antibody specific for HIV-1 Gag p24 and 100 μl of PBS (control) or the sample prepared previously. The wells were incubated for 2 h at room temperature on a horizontal orbital microplate shaker at 500 rpm, washed three times with Wash Buffer and incubated with 200 μl of HIV-1 Gag p24 conjugate for 2 h at room temperature on the shaker. After the incubation, the wells were washed again and incubated with 200 μl of Substrate Solution for 30 min at room temperature protected from the light. The reaction was stopped with 50 μl of Stop Solution and the optical density was measured at 450 nm and corrected at 540 nm in a Synergy HTX multi-mode reader (BioTek).

Methylated RNA immunoprecipitation (MeRIP)

RNA extraction from overexpressing cells (METTL3/14 or FTO) or from cells expressing wild type or GagStop proviral DNA was performed from cells extracts as described above. For MeRIP, 30 μg of total RNA diluted in 380 μl of water was denatured at 70ºC for 5 min and placed on ice for 3 min. The denatured RNA was mixed with 1 μl of rRNasin® (Promega), 5 μl VRC, 100 μl of IP Buffer 5X (50 mM Tris–HCl pH 7.4, 750 mM NaCl and 0.5% NP-40) and 2.5 μl of rabbit polyclonal anti-m^{6}A (1 mg/ml; Abcam #ab151230) and incubated for 2 h at 4ºC with head-over-tail rotation. At the same time, 600 μg of Dynabeads™ Protein A magnetic beads (20 μl; Thermo Fisher) were washed in 1 ml of IP Buffer 1× with 1 μl of VRC and were incubated with 500 μl of Buffer IP 1× with 0.5 mg/ml of BSA for 2 h at 4º C with head-over-tail rotation. Then, beads were washed with 500 μl of IP Buffer 1× and added to the RNA/anti-m^{6}A antibody mix. The RNA-beads mix was incubated for 2 h at 4ºC in head-over-tail rotation. After incubation, the RNA-beads mix was washed twice with 500 μl IP Buffer 1×. Bound RNA was eluted with 100 μl of Elution Buffer (5 mM Tris–HCl pH 7.5, 1 mM EDTA and 0.05% SDS) and 1 μl of Proteinase K (New England BioLabs) and incubated for 1.5 h at 50ºC. RNA was extracted from supernatant using TRIzol™ (Thermo Fisher). The RNA recovered was precipitated with 10 mM $MgCl_2$, 20 μg glycogen (Thermo Fisher) and 2.5 volumes of ETOH 100% overnight at −20ºC and then washed with ETOH 70%. Equal amount of RNA from input and immunoprecipitation (usually 300 ng) were used for RT-qPCR. The full-length RNA from the immunoprecipitated material ('m^{6}A' fraction) was normalized to full-length RNA from the input ('A' fraction). For MeRIP-RT-qPCR analyses using the wild type and the double mutant proviruses, the FL-RNA in the input and the MeRIP samples were normalized to GAPDH.

In the case of the MeRIP-RT-qPCR specific for the 5′-UTR, we generated an *in vitro*-transcribed Renilla luciferase RNA using the T7 RNA polymerase (Promega) in a reaction where rATP was substituted by N^6-methy-ATP (Jena Bioscence). The methylated Renilla luciferase RNA (1 ng) was mixed with the RNA from viral particles and SupT1 infected cells. The RNA mixed was fragmented using Fragmentation Reagent (Thermo Fisher) for 15 min at 70ºC and immunoprecipitated with rabbit polyclonal anti-m^{6}A, as described above. For the RT-qPCR, we used specific primers for the HIV-1 5′-UTR and Renilla luciferase to normalize the level of m^{6}A 5′-UTR RNA in cells and viral particles (Supplementary Table 5).

Prediction of methylated residues

Prediction of methylated adenosines within the 5′-UTR (nucleotides 1–336) of the NL4.3 strain was performed with the SRAMP software available at www.cuilab.cn/sramp considering secondary RNA structure (36).

RNA stability

The stability of the cytoplasmic full-length RNA from control and METTL3/14 overexpressing cells was performed in the presence 20 nM leptomycin B (LMB). Cytoplasmic fractions were collected every hour during a 7-h period following the fractionation protocol described above. The level of the HIV-1 full-length RNA and GADPH at each time point was evaluated by RT-qPCR as described above using primers described in Supplementary Table 4.

Fluorescent in situ hybridization, immunofluorescence and confocal microscopy

Specific probes against the HIV-1 full-length RNA were generated by *in vitro* transcription using the pBSK-Gag/Pol vector and digoxin-11-UTP (Roche) as we previously described (27). The generated 5-kb transcript complementary to the Gag/Pol region of the full-length RNA was fragmented using the RNA fragmentation buffer (Thermo Scientific) to obtain probes of 100–200 nt in length following the supplier 's instructions. Fragmented probes were purified using the Agencourt AMPure XP magnetic beads (Beckman Coulter). RNA FISH was carried out as we recently described (27). Briefy, HeLa cells were cultured in a 12-well plate with coverslips and maintained as described in Methods. Cells were transfected with 0.3 μg of pNL4.3, 0.3 μg of pCMV-VSVg and 1 μg of the corresponding expression vectors as indicated in Materials and Methods. At 24 hpt, cells were washed twice with 1× PBS and fixed for 10 min at room temperature with 4% paraformaldehyde. Cells were subsequently permeabilized for 10 min at room temperature with 0.2% Triton X-100 and hybridized overnight at 37ºC in 200 μl of hybridization mix (10% dextran sulfate, 2 mM VRC, 0.02% RNase-free BSA, 50% formamide, 300 μg tRNA and 120 ng of 11-digoxigenin-UTP probes) in a humid chamber. Cells were washed with 0.2× SSC/50% formamide during 30 min at 50ºC and then incubated three times with antibody dilution buffer (2× SSC, 8% formamide, 2 mM vanadyl-ribonucleoside complex, 0.02% RNase-free BSA). Sheep anti-digoxin (Roche), mouse HIV-1 anti-p24 (NIH AIDS Reagents Program, Catalog number 3537) and Rabbit anti-Flag (Sigma) primary antibodies diluted to 1/100 in antibody dilution buffer were added for 2 h at room temperature. After three washes with antibody dilution buffer, cells were incubated for 90 min at room temperature with anti-Sheep Alexa 488, anti-mouse Alexa 594 and anti-rabbit Alexa 647 antibodies (Molecular Probes) diluted at 1/500. Cells were washed three times in wash buffer (2× SSC, 8% formamide, 2 mM vanadyl-ribonucleoside

Downloaded from https://academic.oup.com/nar/article/50/4/2302/6524254 by guest on 11 April 2024

complex), twice with 1× PBS, incubated with DAPI (0.3 μg/ml in PBS) (Life Technologies) for 1 min at room temperature, washed three times with 1X PBS, three times with water and mounted with Fluoromount™ (Life Technologies). Images were obtained with a Zeiss LSM 800 Confocal Microscope (Zeiss) and processed using FIJI/ImageJ (NIH).

Proximity ligation (PLA)

PLA was carried out using the DUOLINK II In Situ kit (Sigma-Aldrich) and PLA probe anti-mouse minus and PLA probe anti-rabbit plus (Sigma-Aldrich) as we have previously described (27). Briefly, HeLa cells transfected with pNL4.3 and pCDNA-3XFlag-FTO for 24 h were fixed and pre-incubated with blocking agent for 30 min at room temperature. Primary antibodies were added at a dilution of 1/100 (mouse anti-HIV-1 p24 monoclonal antibody) and 1/200 (rabbit anti-Flag, Sigma-Aldrich) in 40 μl DUOLINK antibody diluent and incubated at 37ºC for 1 h. Samples were washed three times with PBS for 5 min each and secondary antibodies (DUOLINK anti-rabbit PLA-plus probe and DUOLINK anti-mouse PLA-minus probes) were added and incubated at 37ºC for 1 h. Ligation and amplification reactions were performed following the same protocol described in (27). Samples were incubated with DAPI (0.3 μg/ml in PBS) (Life Technologies) for 1 min at room temperature and coverslips were washed three times with PBS, three times with water and mounted with Fluoromount™ (Sigma Aldrich). Images were obtained with a Zeiss LSM 800 Confocal Microscope (Zeiss) and processed using FIJI/ImageJ (NIH).

In situ hybridization coupled to PLA (ISH-PLA)

The ISH-PLA protocol was developed by mixing the RNA-FISH and PLA protocols described above essentially as we have previously reported (37). Briefly, HeLa cells transfected with pNL4.3 and pCDNA-Flag-METTL3 or pCDNA-3XFlag-FTO growing on coverslips were fixed, permeabilized for 10 min at RT with 0.2% Triton X-100 and hybridized overnight at 37ºC in 200 μl of hybridization mix (10% dextran sulphate, 2 mM vanadyl–ribonucleoside complex, 0.02% RNase-free bovine serum albumin, 50% formamide, 300 μg of tRNA and 120 ng of 11-digoxigenin-UTP probes) in a humid chamber. Cells were washed with 0.2× SSC/50% formamide during 30 min at 50ºC and incubated with blocking agent for 30 min to room temperature. Cells were then incubated three times with antibody dilution buffer (2× SSC, 8% formamide, 2 mM vanadyl–ribonucleoside complex and 0.02% RNase-free bovine serum albumin). Mouse anti-digoxin and rabbit anti-flag primary antibodies diluted to 1/100 in antibody dilution buffer were added for 2 h at room temperature. After three washes with antibody dilution buffer and two washes with PBS for 5 min each, the secondary antibodies (DUOLINK anti-rabbit PLA-plus probe, DUOLINK anti-mouse PLA minus probe) were added and incubated at 37ºC for 1 h. The ligation and amplification reactions were performed following the same protocol described above. Thereafter, coverslips were incubated with a solution of DAPI (0.3 μg/ml in PBS) (Life Technologies) for 1 min at room temperature, washed three times with PBS, three times with water and mounted with Fluoromount™ (Sigma Aldrich). Images were obtained with a Zeiss LSM 800 Confocal Microscope (Zeiss) and processed using FIJI/ImageJ (NIH).

Subcellular fractionation

Cells expressing HIV-1 NL4.3 were recovered, washed with ice-cold 1× PBS and centrifuged at 500 × g at RT for 5 min followed by a second wash with ice-cold 1× PBS and a centrifugation at 10 000 rpm for 10 s at 4°C. Then, cell pellet was resuspended in 300 μl of lysis buffer (10 mM HEPES, 10 mM NaCl, 3 mM $CaCl_2$, 0.1% Nonidet-P40 and 1× protease inhibitors cocktail) by pipetting up and down 5 times and the lysate was centrifuged at 10 000 rpm for 10 s at 4°C. The supernatant containing the cytoplasmic fraction was transferred to a new tube and the nuclear pellet was washed twice by resuspending in lysis buffer and the supernatant was discarded. Nuclear fraction was lysed in 100 μl lysis buffer (100 mM NaCl, 10 mM Tris–HCl pH 7.5, 0.5% Nonidet-P40, 1 mM EDTA and 1× protease inhibitors cocktail). Cytoplasmic and nuclear fraction were cleared by centrifugation at 13 000 rpm for 5 min at 4°C and the supernatant was quantified by the Bradford assay (Bio-Rad). Levels of HIV-1 Gag, nucleolin and tubulin were evaluated by western blot as described above using the following antibodies: C23 (MS-3; sc-8031 Santa Cruz Biotechnologies), β-tubulin (e-10; sc-365791 Santa Cruz Biotechnologies) and p24 (NIH) at a 1/1000 dilution.

Electron microscopy

HIV-1-expressing cells under control and METTL3/14 overexpression conditions were fixed with 2.5% glutaraldehyde in 100 mM cacodylate buffer pH 7.2 for 6 h at room temperature and washed with 100 mM sodium cacodylate buffer at pH 7.2 for 18 h at 4ºC. Samples were fixed with 1% aqueous osmium tetroxide for 90 min and soaked with distilled water. Then, cells were stained with 1% aqueous uranyl acetate for 60 min. Samples were dehydrated with 50%, 70%, 95% (twice) and 100% (three times) of acetone, for 20 min each. Samples were embedded in an EPON resin:acetone at 1:1 overnight and then embedded in EPON resin that previously polymerized at 60ºC for 24 h. Fine cuts (60–70 nm) were obtained in a Sorval MT-5000 ultramicrotome, arranged on copper grids, and stained with uranyl acetate 4% in methanol for 2 min and lead citrate for 5 min. Samples were observed with a Philips Tecnai 12 electron microscope at 80 kV.

Adenosine conservation analysis

For the adenosine conservation analysis, all the HIV-1 sequences present in HIV database were aligned with *HIV Premade Aligments*, ALL GENOME options, processed and classified with an *in-house* script. Motifs surrounding A_{198} and A_{242} were analyzed by *WebLogo* v2.8.2 (https://weblogo.berkeley.edu/logo.cgi). A detailed summary of the bioinformatic analyses can be found at the Supplementary materials available at NAR online.

Downloaded from https://academic.oup.com/nar/article/50/4/2302/6524254 by guest on 11 April 2024

RESULTS

The presence of m^{6}A within the full-length RNA favors Gag synthesis but interferes with packaging

In order to study the role of m^{6}A on the cytoplasmic fate of the FL-RNA during viral replication, we first determined the effects of METTL3/14 overexpression on Gag and FL-RNA levels obtained from cell extracts and concentrated viral particles (see scheme in Supplementary Figure S1A). MeRIP-RT-qPCR analysis from METTL3/14 overexpressing cells showed a 3-fold increase in the m^{6}A/A ratio of the FL-RNA compared to the control condition indicating an increase in the content of m^{6}A in the viral transcript under these experimental conditions (Supplementary Figure S1B). Consistent with the positive role of m^{6}A on Gag synthesis previously described (23–25), we observed that increased methylation of the FL-RNA by METTL3/14 overexpression results in increased levels of intracellular Gag and its processing products that were accompanied by a 20% reduction in the total intracellular FL-RNA (Figure 1A). Quantification of viral particles produced from the same cells revealed a slight increase in Gag levels (as judged by anti-CAp24 ELISA) from METTL3/14 overexpressing cells, which could be attributed to the increased intracellular Gag levels observed (Figure 1B, left panel). Then, we quantified the FL-RNA from equivalent amounts of CAp24 and observed that viral particles produced under METTL3/14 overexpression contain around 3-fold less packaged FL-RNA suggesting that methylation of the FL-RNA by METTL3/14 inhibits packaging (Figure 1B, right panel). Since HIV-1 virions were shown to contain 3 000 to 11 000 molecules of Gag resulting in 119–207 nm viral particles (38), we looked at the size of particles released from control or METTL3/14 overexpressing cells in order to verify that the reduction of the packaged FL-RNA observed is not due to an increase in the number of Gag molecules per virion. Of note, we were not able to identify changes in particle size that could explain the differences observed in the packaged FL-RNA (Supplementary Figure S1C), further indicating that hypermethylation of the viral RNA impedes its packaging into nascent particles. Interestingly, we observed that METTL3/14 overexpression results in a slight reduction of the half-life of the FL-RNA in the cytoplasm from 2.2 ($R^2 = 0.9277$) to 1.6 ($R^2 = 0.9329$) hours suggesting that the presence of m^{6}A might induce an accelerated metabolism of the viral RNA (Supplementary Figure S1D). Consistent with an important role of m^{6}A on Gag synthesis, METTL3 knockdown by a previously described short hairpin RNA resulted in decreased intracellular Gag levels without changes in the total FL-RNA (Figure 1C). Moreover, we observed a small yet significant decrease in the released particles, which was associated with an important increase in the packaged FL-RNA, thus confirming the critical role of m^{6}A in defining the cytoplasmic fate of this viral RNA (Figure 1D).

Since results presented above suggest that m^{6}A deposition by METTL3/14 affects the cytoplasmic fate of the FL-RNA, we wanted to investigate where within the cell the m^{6}A writer complex modifies the viral RNA. For this, we analyzed the interaction between the FL-RNA and METTL3 by *in situ* hybridization coupled to the proximity ligation assay (ISH-PLA), which we have successfully used to quantify FL-RNA-protein interactions in intact cells (27,37). Confocal microscopy analyses revealed a predominant interaction within the nucleus, which suggests that the FL-RNA must be methylated in the nucleus and reach the cytoplasm in a methylated form (Figure 1E and Supplementary Figure S1E). We also employed the ISH-PLA strategy to investigate the interaction between the FL-RNA and Gag under control and METTL3/14 overexpression conditions. Interestingly, we observed a significant decrease in the FL-RNA-Gag interaction under METTL3/14 overexpression suggesting that FL-RNA methylation may directly or indirectly interfere with Gag binding (Figure 1F and Supplementary Figure S1F).

Together, these data suggest that methylation of the HIV-1 FL-RNA by the METTL3/14 complex favors its use as mRNA for Gag synthesis but interferes with its incorporation into viral particles.

Packaged full-length RNA lacks m^{6}A residues at the 5′-UTR

From data presented above, it seems that the presence of m^{6}A interferes with the function of the HIV-1 FL-RNA as genomic RNA. Thus, to gain further insights into this regulation, we employed the MeRIP-seq strategy to determine the m^{6}A patterns of the intracellular and viral particle-associated HIV-1 FL-RNA. In agreement with previous data reported for the NL4.3 and LAI.2 strains in T-lymphocytes and HEK293T cells (23–25), we identified an m^{6}A peak at the 5′-UTR and a cluster of peaks at the 3′ end of the intracellular FL-RNA (Figure 2A and Supplementary Figure S2A, see intracellular FL-RNA). Interestingly, we observed that the FL-RNA from purified viral particles maintains the cluster of m^{6}A peaks at the 3′-UTR but lacks the m^{6}A peak at the 5′-UTR. This observation together with data from Figure 1 suggests that the presence of m^{6}A at the 5′-UTR interferes with the incorporation of the FL-RNA into viral particles (Figure 2A and Supplementary Figure S2A, see virion FL-RNA). Of note, this difference in the methylation patterns between intracellular and packaged RNA was not observed in the host 7SL RNA, which is also packaged at high levels into HIV-1 particles (39,40), indicating a very specific effect of m^{6}A on FL-RNA packaging (Supplementary Figure S2B). To confirm this observation, we infected SupT1 T-lymphocytes and employed MeRIP-RT-qPCR to quantify the methylation status of the 5′-UTR in the FL-RNA present within the cell and in concentrated viral particles. In agreement with our MeRIP-seq data obtained in HEK293T cells, we observed a dramatic decrease in the m^{6}A/A ratio of the 5′-UTR in the FL-RNA obtained from viral particles further indicating that the viral particle-associated RNA preferentially lacks m^{6}A residues at the 5′-UTR (Figure 2B). These data strongly suggest that FL-RNA molecules lacking m^{6}A at the 5′-UTR are primarily selected by Gag as gRNA to be incorporated into viral particles.

Adenosine residues 198 and 242 are key for efficient packaging of the full-length RNA

Considering the critical role of the 5′-UTR in FL-RNA packaging, we then sought to determine whether specific

Downloaded from https://academic.oup.com/nar/article/50/4/2302/6524254 by guest on 11 April 2024

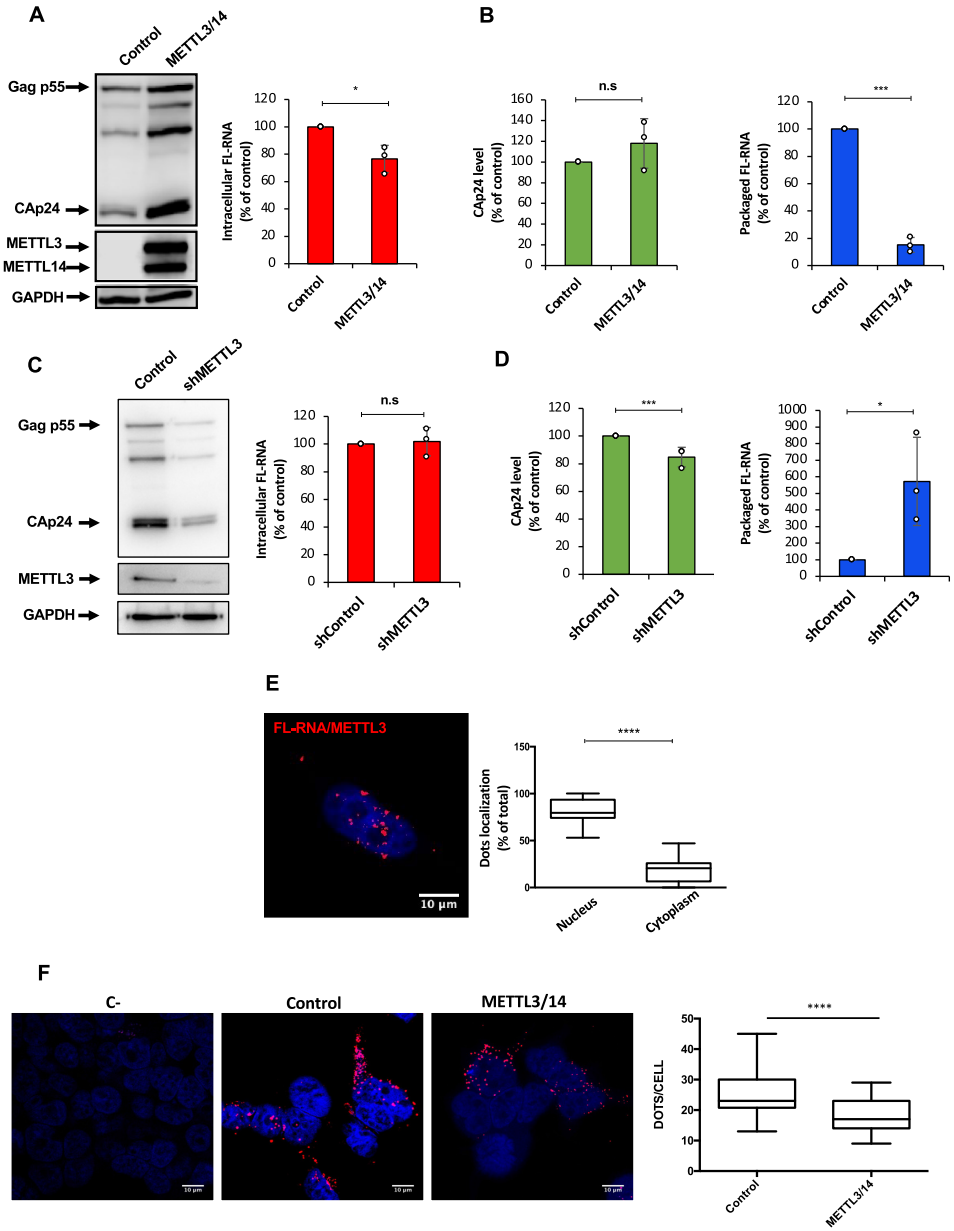

Figure 1. The presence of m^{6}A within the full-length RNA favors Gag synthesis but interferes with packaging. HEK293T cells were transfected with pNL4.3 and pCMV-VSVg together with pCDNA-Flag-METTL3 and pCDNA-Flag-METTL14 or pCDNA-d2EGFP as a control. (**A**) At 24 hpt cells extracts were used to detect Gag, Flag-METTL3 and Flag-METTL14 by Western blot. GAPDH was used as a loading control (left panel). In parallel, cells extracts were used to perform RNA extraction and the full-length RNA was quantified by RT-qPCR (right panel). Intracellular full-length RNA was normalized to the control (arbitrary set to 100%) and presented as the mean ± SD of three independent experiments (*$P < 0.05$, *t*-test). (**B**) Supernatants from cell cultures in (A) were filtered and viral particles were purified by ultracentrifugation. The level of CAp24 was quantified by an anti-CAp24 ELISA. The level of CAp24 was normalized to the control (arbitrary set to 100%) and presented as the mean ± SD of three independent experiments (ns; non-significant, *t*-test) (left panel). Viral particles purified were used to perform RNA extraction and the packaged full-length RNA from CAp24 equivalents was quantified by RT-qPCR. Packaged full-length RNA was normalized to the control (arbitrary set to 100%) and presented as the mean ± SD of three independent experiments (right panel). (**C**) METTL3 knockdown HEK293T cells were transfected with pNL4.3 and pCMV-VSVg. At 24 hpt cells extracts were used to detect Gag, METTL3 and GAPDH by Western blot. (**D**) Supernatant from cell cultures were filtered and viral particles were purified by ultracentrifugation. The level of CAp24 was quantified by an anti-CAp24 ELISA and the packaged full-length RNA from CAp24 equivalents was quantified by RT-qPCR. Packaged full-length RNA was normalized to the control (arbitrary set to 100%) and presented as the mean ± SD of three independent experiments. (*$P < 0.05$; ***$P < 0.001$, *t*-test). (**E**) HeLa cells were transfected with pNL4.3, pCMV-VSVg and pCDNA-Flag-METTL3. At 24 hpt, the interaction between full-length RNA and Flag-tagged METTL3 was analyzed by ISH-PLA as described in the Materials and Methods section. Red dots indicate the interactions between the full-length RNA and Flag-METTL3. Scale bar 10 mm. A quantification of the red dots in the nucleus (co-localizing with the DAPI staining) and the cytoplasm is presented on the right (****$P < 0.0001$, Mann–Whitney test). (**F**) HeLa cells were transfected with pNL4.3, pCMV-VSVg, pCDNA-Flag-METTL3 and pCDNA-Flag-METTL14. At 24 hpt, the interaction between the full-length RNA and Gag was analyzed by ISH-PLA as described in the Materials and Methods section. Red dots indicate the interactions between the full-length RNA and Gag. Scale bar 10 mm. A quantification of the red dots in both conditions is presented on the right (****$P < 0.0001$, Mann–Whitney test).

Downloaded from https://academic.oup.com/nar/article/50/4/2302/6524254 by guest on 11 April 2024

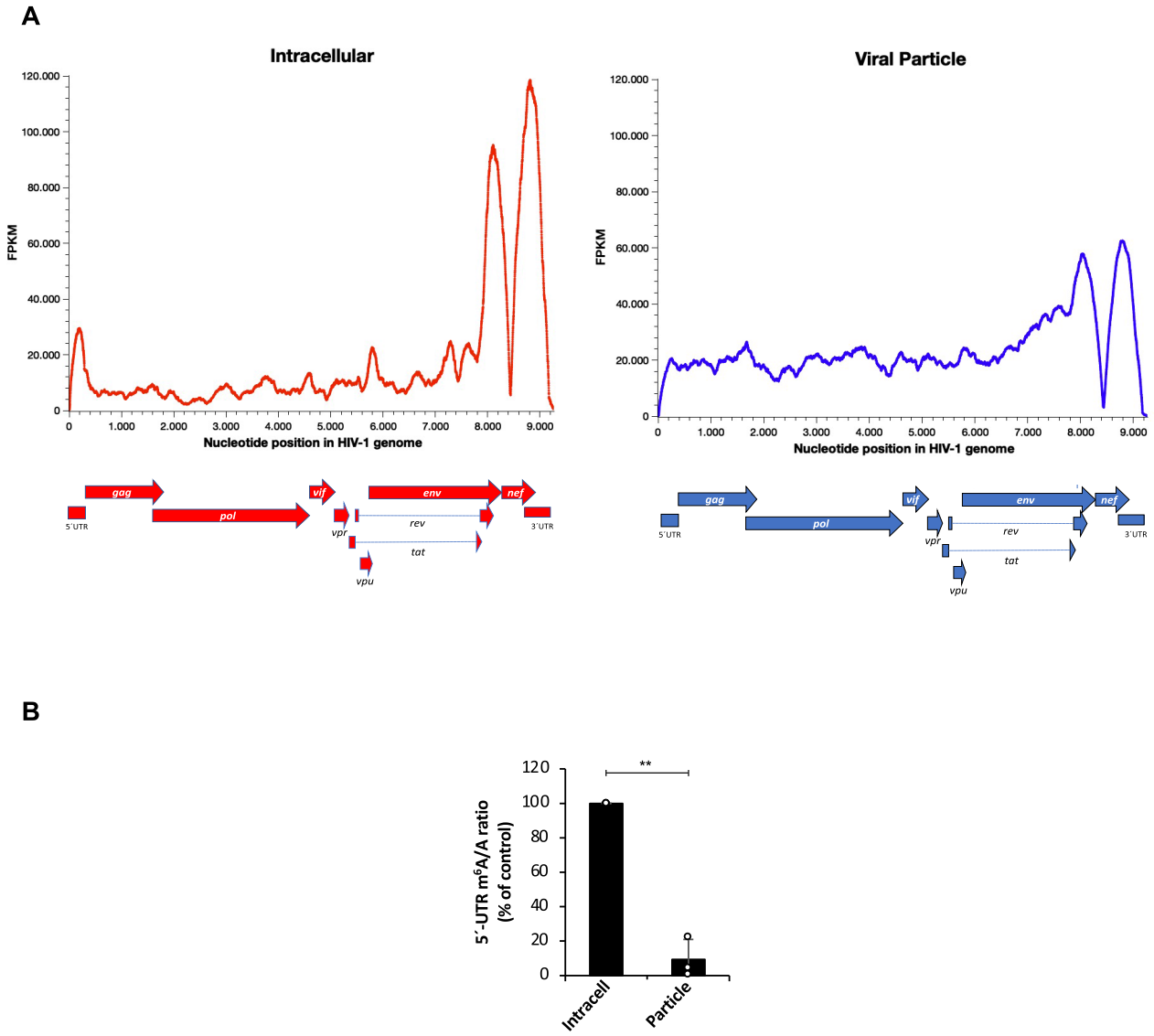

Figure 2. Packaged full-length RNA lacks m^6A residues at the 5′-UTR. (**A**) HEK293T cells were transfected with pNL4.3 and pCMV-VSVg. Intracellular polyA RNA or viral particle-associated RNA was extracted at 24 hpt, fragmented and used for MeRIP-seq as described in Materials and Methods section. Peak calling plots for the intracellular (left) and packaged (right) full-length RNA are shown. The drop in the peak near the beginning of the Nef coding region corresponds to the site where the EGFP-Puro cassette is inserted. (**B**) SupT1 cells were infected with HIV-1 NL4.3 pseudotyped with VSVg. At 24 hpi, supernatants were filtered, and viral particles were concentrated by ultracentrifugation. The RNA from cells and viral particles were used to perform a MeRIP-RT-qPCR specific for the 5′-UTR as described in the Materials and Methods section.

adenosine residues at this region were involved in the regulation of FL-RNA packaging by METLL3/14. As a first approach, we performed a bioinformatic prediction and identified A_{198} and A_{242} (numbering considering the ^{Cap}2G FL-RNA as described in (41–43)) within the 5-UTR of the NL4.3 strain as the potentially methylated residues (Supplementary Figure S3A). In addition, both residues are contained within the m^6A peak we have mapped around nucleotides 80 and 283 within the 5′-UTR of the intracellular FL-RNA (Supplementary Figure S3B and Supplementary Table 2) that was also identified in previous MeRIP-seq data obtained from T-lymphocytes and HEK293T cells (23–25). Since both residues are predicted to locate in loops rather than base-paired regions (44), we deleted A_{198}, A_{242} or both from the NL4.3 provirus to analyze the role of these two adenosine residues on the m^6A-mediated regulation of FL-RNA packaging. We first observed that the $\Delta A_{198}/\Delta A_{242}$ double mutant presented higher levels of Gag when compared to the wild type and single mutant proviruses suggesting that both residues might act together to promote Gag synthesis (Figure 3A). Interestingly, while both single mutant viruses showed no significant differences in CAp24 levels and packaged FL-RNA, the $\Delta A_{198}/\Delta A_{242}$ mutant presented a significant reduction in released particles and a 2.5-fold reduction in FL-RNA packaging further suggesting that both adenosine residues act together in the regulation of FL-RNA metabolism (Figure 3B). These observations prompted us to further ana-

Downloaded from https://academic.oup.com/nar/article/50/4/2302/6524254 by guest on 11 April 2024

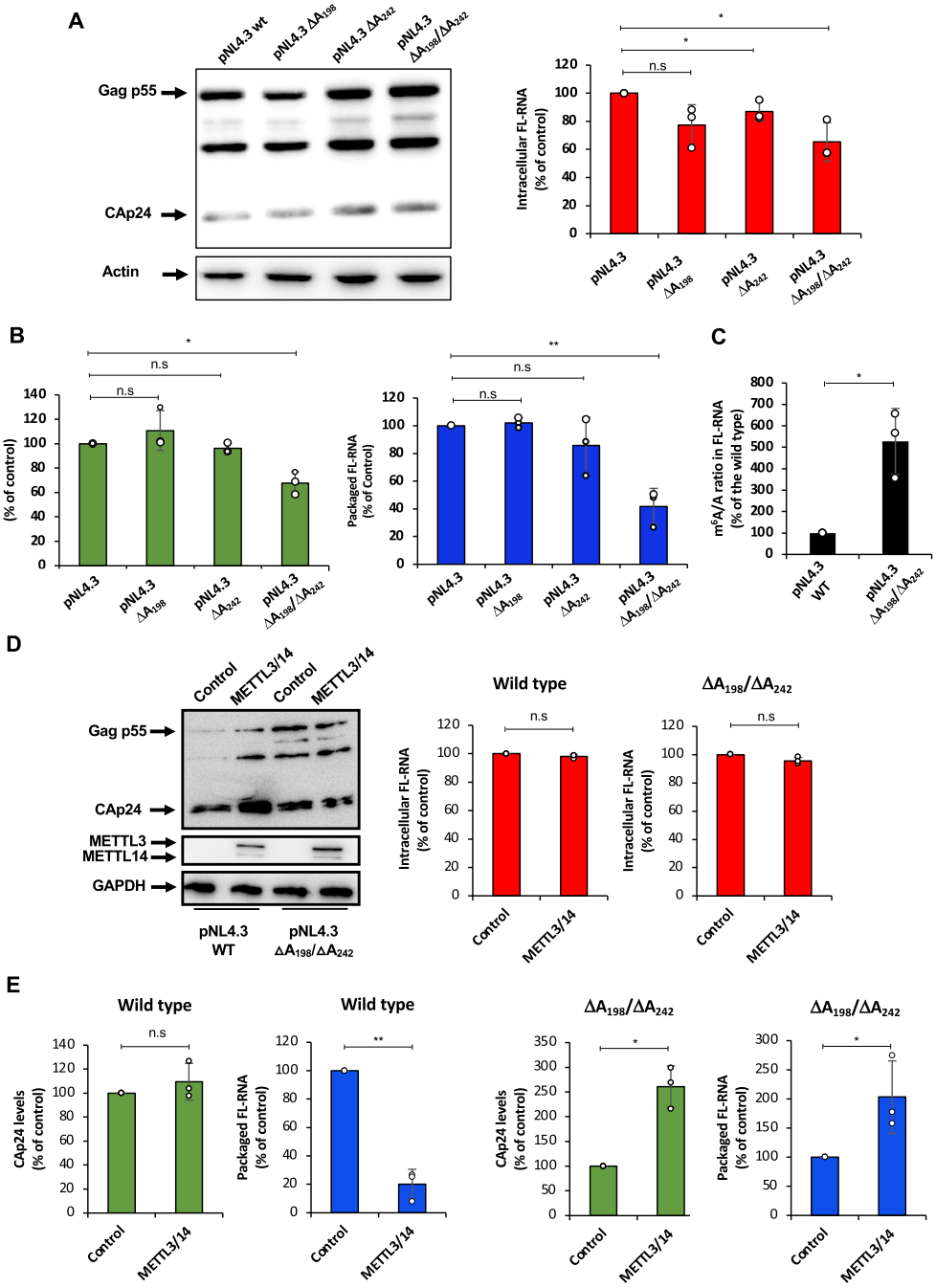

Figure 3. Adenosine residues 198 and 242 are key for HIV-1 full-length RNA packaging. (**A**) HEK293T cells were transfected with pNL4.3 wild type, pNL4.3 ΔA_{198}, pNL4.3 ΔA_{242} or pNL4.3 $\Delta A_{198}/\Delta A_{242}$ together with pCMV-VSVg. At 24 hpt, cells extracts were used to detect Gag by Western blot. Actin was used as a loading control (left panel). In parallel, cells extracts were used to perform RNA extraction and the full-length RNA was quantified by RT-qPCR (right panel) (*$P < 0.05$; ns; non-significant, *t*-test). (**B**) The supernatant from (A) was filtered and concentrated viral particles were used to perform anti-CAp24 ELISA and RNA extraction for RT-qPCR analysis. The levels of CAp24 and the packaged full-length RNA (per CAp24 equivalents) were normalized to the wild type provirus (arbitrary set to 100%) and presented as the mean ± SD of three independent experiments (*$P < 0.05$; ns; non-significant, *t*-test). (**C**) HEK293T cells were transfected with pNL4.3 wild type or pNL4.3 $\Delta A_{198}/\Delta A_{242}$ together with pCMV-VSVg. At 24 hpt the RNA from cells was used to perform a MeRIP-RT-qPCR as described in the Materials and Methods section (*$P < 0.05$; n.s, *t*-test). (**D**) HEK293T cells were transfected with pNL4.3 wild type or pNL4.3 $\Delta A_{198}/\Delta A_{242}$ together with pCMV-VSVg, pCDNA-Flag-METTL3 and pCDNA-Flag-METTL14 or pCDNA-d2EGFP as a control. At 24 hpt cells extracts were used to detect Gag, Flag-METTL3 and Flag-METTL14 by Western blot. GAPDH was used as a loading control (left panel). In parallel, cells extracts were used to perform RNA extraction and the full-length RNA was quantified by RT-qPCR (right panel). Intracellular full-length RNA was normalized to the control (arbitrary set to 100%) and presented as the mean ± SD of three independent experiments (ns; non-significant, *t*-test). (**E**) At 24 hpt supernatants were filtered and viral particles were concentrated by ultracentrifugation. Purified viral particles were used to perform an anti-CAp24 ELISA and RNA extraction and RT-qPCR analysis. The levels of CAp24 and the packaged full-length RNA (per CAp24 equivalents) were normalized to the control (arbitrary set to 100%) and presented as the mean ± SD of three independent experiments (*$P < 0.05$; **$P < 0.01$; ns, non-significant, *t*-test).

Downloaded from https://academic.oup.com/nar/article/50/4/2302/6524254 by guest on 11 April 2024

lyze the impact of the $\Delta A_{198}/\Delta A_{242}$ double mutant provirus on the m^{6}A-mediated regulation of FL-RNA packaging. A rather surprising observation was that the FL-RNA from the $\Delta A_{198}/\Delta A_{242}$ mutant contains around 5-fold more m^{6}A levels when compared to the wild type FL-RNA suggesting that m^{6}A methylation of these two adenosines is not directly involved in the regulation of FL-RNA packaging but these residues are important for the regulation of the overall m^{6}A levels of the viral transcript (Figure 3C). The increased m^{6}A content in the FL-RNA containing the $\Delta A_{198}/\Delta A_{242}$ mutation might explain both the increased Gag levels and reduced FL-RNA packaging, which is similar to what we observed above with the wild type provirus under METTL3/14 overexpression. Indeed, despite the $\Delta A_{198}/\Delta A_{242}$ mutant provirus accumulates more intracellular Gag compared to the wild type, this level was not further increased by METTL3/14 overexpression as occurs with the wild type virus (Figure 3D). In addition, while FL-RNA packaging of the wild type provirus was strongly inhibited under METTL3/14 overexpression, the inefficient packaging of the FL-RNA from the double mutant provirus observed in Figure 3A presented a 2-fold increase under similar conditions (Figure 3E). Consistent with A_{198} and A_{242} acting together rather than independently in the m^{6}A-mediated regulation of FL-RNA packaging, we observed that ΔA_{198} and ΔA_{242} single mutant proviruses were still susceptible to the negative effect of METTL3/14 overexpression on FL-RNA packaging as observed with the wild type provirus (Supplementary Figure S3C).

In addition to A_{198} and A_{242}, residues A_{16}, A_{47}, A_{55}, A_{124}, A_{133}, A_{149}, A_{192} and A_{311} within the 5′-UTR of the NL4.3 FL-RNA are also in the DRACH context and could be important for this m^{6}A-mediated regulation. An analysis of 890 sequences from the HIV database (www.hiv.lanl.gov), including the highly prevalent subtypes C and B as well as circulating recombinant forms, indicate that all these adenosines with the exception of A_{47} are present in a highly conserved DRACH methylation context suggesting that the epitranscriptomic regulation observed could be a common feature of different HIV-1 subtypes (Supplementary Figure S3D and S3E).

Together, these data suggest that adenosine residues 198 and 242 together play an important role in regulating the overall m^{6}A levels of the FL-RNA and therefore, its ability to function as mRNA or the packaged genome.

Demethylation by a Gag-FTO complex favors HIV-1 full-length RNA packaging

Then, we sought to determine whether this m^{6}A-mediated regulation of FL-RNA packaging was a dynamic process. This was important considering that the reversible nature of adenosine methylation in cellular mRNA has been challenged (45). For this, we overexpressed the RNA demethylase FTO and the analysis of the m^{6}A/A ratio of the FL-RNA in control and FTO overexpressing cells revealed that the viral RNA is indeed a substrate for this m^{6}A eraser (Supplementary Figure S4A). We observed that FTO-induced demethylation of the FL-RNA has no significant effects on intracellular Gag and FL-RNA levels (Figure 4A). Consistent with no changes in intracellular Gag levels, we also observed no changes in the CAp24 levels from purified viral particles produced under FL-RNA demethylation conditions (Figure 4B, left panel). However, and in agreement with a negative role of m^{6}A on FL-RNA packaging, we observed that viral particles produced from FTO overexpressing cells contain around 5-fold more packaged FL-RNA compared to the control (Figure 4B, right panel). It should be mentioned that we were not able to observe such a strong effect on FL-RNA packaging when the RNA demethylase ALKBH5 was overexpressed suggesting that FL-RNA demethylation by FTO is important for packaging (Supplementary Figure S4B).

Considering that m^{6}A demethylation favors FL-RNA packaging, we wanted to know where within the cell the viral RNA became demethylated by FTO. For this, we analyzed the interaction between the FL-RNA and FTO in cells by ISH-PLA but despite several attempts, we were not able to detect a direct interaction regardless all the components were correctly expressed within the cells (Supplementary Figure S4C). This observation suggests that either there is not a massive interaction between the FL-RNA and FTO, that such interactions occur very transiently (or at very low rates) being below the detection limit of our ISH-PLA strategy or that the FTO-binding site within the FL-RNA is not close enough to the sites where our probes hybridize (Gag-Pol region) thus, impeding the PLA reaction.

The lack of a detectable interaction between the FL-RNA and FTO prompted us to investigate whether Gag could interact with FTO and participate in FL-RNA demethylation. To test this possibility, we employed the proximity ligation assay (PLA) and observed that Gag and FTO indeed form complexes in intact cells (Figure 4C). Interestingly, quantification of the dots per cell localizing with the nuclear staining as well as 3D reconstitutions of representative images indicate that Gag and FTO mostly associate within the nucleus (Figure 4D and E). Since the presence of HIV-1 Gag in the nucleus has been controversial, we prepared nuclear and cellular fractions from HIV-1 expressing cells and analyzed the localization of Gag. Consistent with previous studies performed with HIV-1 and Rous sarcoma virus (46–49), we detected the presence of a small proportion of Gag in nuclear fractions (Supplementary Figure S4D).

From these results, it was tempting to speculate that the FL-RNA is methylated within the nucleus by METLL3/14 and Gag interacts with FTO in the nucleus to promote demethylation of the FL-RNA molecules that will be incorporated into assembling viral particles. To further validate this last idea, we analyzed the m^{6}A content of the FL-RNA in the presence or absence of Gag by using the wild type NL4.3 provirus and a mutant provirus containing premature stops codons that abolish Gag synthesis (GagStop provirus). We also included a condition in which the GagStop provirus was co-expressed together with a Gag expressing vector. Despite we detected similar levels of FL-RNA in all the conditions tested, the Gag polyprotein was only detected in samples from cells expressing the wild type virus or the Gag-expressing vector, as expected (Figure 4F, left and middle panels). Compared to the wild type FL-RNA, the level of m^{6}A increases when Gag is absent and is restored or even decreased when the Gag protein was ex-

Downloaded from https://academic.oup.com/nar/article/50/4/2302/6524254 by guest on 11 April 2024

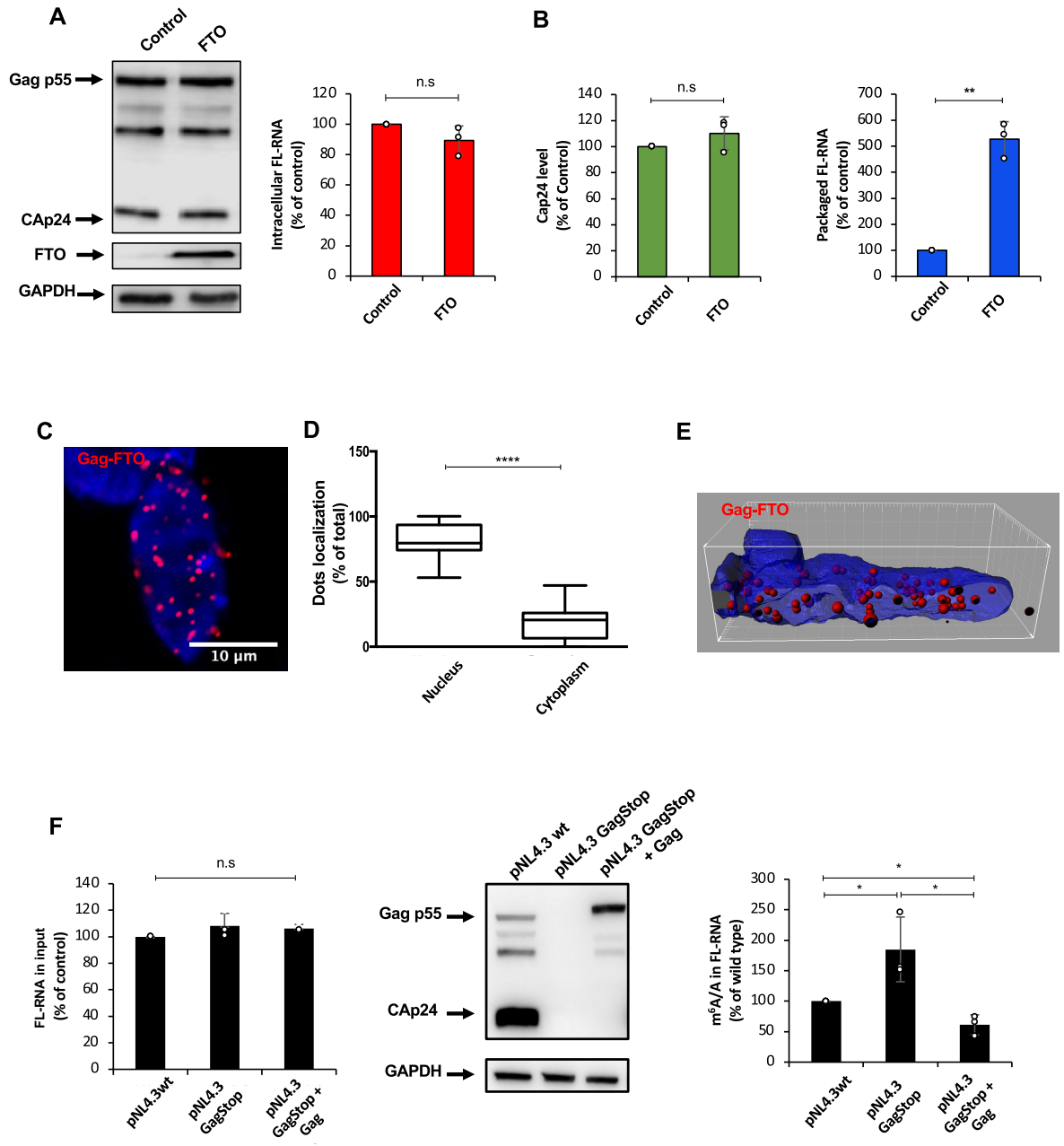

Figure 4. Demethylation by a Gag-FTO complex favors HIV-1 full-length RNA packaging. (**A**) HEK293T cells were transfected with pNL4.3 and pCMV-VSVg together with pCDNA-3XFlag-FTO or pCDNA-3XFlag-d2EGFP as a control. At 24 hpt cells extracts were used to detect Gag and 3XFlag-FTO by Western blot. GAPDH was used as a loading control (left panel). In parallel, cells extracts were used to perform RNA extraction and the full-length RNA was quantified by RT-qPCR (right panel). Intracellular full-length RNA was normalized to the control (arbitrary set to 100%) and presented as the mean ± SD of three independent experiments (*$P < 0.05$, *t*-test). (**B**) Supernatants from cell cultures in (A) were filtered and viral particles were concentrated by ultracentrifugation. The level of CAp24 was quantified by an anti-CAp24 ELISA, normalized to the control (arbitrary set to 100%) and presented as the mean ± SD of three independent experiments (n.s; non-significant, *t*-test) (left panel). Viral particles were used to perform RNA extraction and the packaged full-length RNA from CAp24 equivalents was quantified by RT-qPCR. Packaged full-length RNA was normalized to the control (arbitrary set to 100%) and presented as the mean +/− SD of three independent experiments (**$P < 0.01$, *t*-test) (right panel). (**C**) HeLa cells were co-transfected with pNL4.3, pCMV-VSVg and pCDNA-3XFlag-FTO. At 24 hpt, the interaction between Gag and Flag-tagged FTO was analyzed by PLA as described in Materials and Methods section. Red dots indicate the interactions between Gag and FTO (left panel). Scale bar 10 mm. (**D**) Three-dimensional reconstitution of the PLA results shown in (C) was performed to determine the subcellular localization of the interaction between Gag and FTO. (**E**) Quantification of the red dots in the nucleus (co-localizing with the DAPI staining) and the cytoplasm of 15 cells is presented on the right (****$P < 0.0001$, Mann–Whitney test). (**F**) HEK293T cells were transfected with the pNL4.3 wild type, pNL4.3-GagStop or pNL4.3-GagStop together with pCDNA-Gag. At 24 hpt cells extracts were used to detect Gag and GAPDH was used as a loading control. In parallel, cells extracts were used to perform RNA extraction followed by an immunoprecipitation using an anti-m^{6}A antibody (MeRIP-RT-qPCR as described in Materials and Methods section). The full-length RNA from the input was quantified by RT-qPCR (left panel). The full-length RNA from the input ('A' fraction) and from the immunoprecipitated material ('m^{6}A' fraction) was quantified by RT-qPCR. The m^{6}A/A ratio was normalized to pNL4.3 wild type (arbitrary set to 100%) and presented as the mean ± SD of three independent experiments (*$P < 0.05$, *t*-test).

Downloaded from https://academic.oup.com/nar/article/50/4/2302/6524254 by guest on 11 April 2024

pressed *in trans* indicating that Gag regulates the methylation status of the FL-RNA (Figure 4F, right panel).

Together, these results strongly suggest that the FTO-mediated demethylation is required for FL-RNA packaging in a process supported by the Gag precursor.

Inhibition of FTO demethylase activity impacts full-length RNA metabolism and blocks packaging

We finally sought to determine whether this epitranscriptomic regulation of the HIV-1 FL-RNA packaging was a potential therapeutic target for pharmacological intervention. For this, we took advantage of the ester form of meclofenamic acid (MA2), which was shown to specifically interfere with FTO-mediated m^{6}A demethylation (50). Therefore, we analyzed Gag and the FL-RNA in cells treated with MA2 (DMSO as a control) and observed a reduction in Gag synthesis and the intracellular levels of the FL-RNA indicating that FTO-mediated demethylation is required for proper metabolism of the FL-RNA within the cell (Figure 5A). Consistent with a perturbed intracellular FL-RNA metabolism, we observed a decrease in the viral particles released from MA2-treated cells (Figure 5B, left panel). Strikingly, quantification of the packaged FL-RNA from equal amounts of viral particles indicates that inhibition of FTO activity by MA2 almost abolished packaging (Figure 5B, right panel). Finally, and to gain further insights into the role of A_{198} and A_{242} on FL-RNA packaging, we analyzed the impact of MA2 in the double mutant provirus. Similar to the wild type provirus, we observed that MA2 treatment reduces the intracellular levels of Gag and the FL-RNA suggesting that the impact of MA2 on viral gene expression is independent of the presence of A_{198} and A_{242} in the 5′-UTR (Figure 5C). In agreement with reduced intracellular Gag, we also observed a decrease in the levels of viral particles released from MA2-treated cells (Figure 5D, left panel). However, and in contrast with what we observed with the wild type provirus, treatment with MA2 slightly stimulated FL-RNA packaging of the double mutant provirus (Figure 5D, right panel).

Together, these results provide further evidence for a role of FTO-mediated demethylation as an important step for HIV-1 FL-RNA packaging and this process is a potential target for the design of novel antiretroviral drugs.

DISCUSSION

Assembly of human immunodeficiency virus type-1 particles is a highly regulated process in which the major structural polyprotein Gag together with other viral and cellular components are recruited to the plasma membrane for the release of the viral progeny. The assembly process occurs in multiple steps driven by the different functional domains that compose the Gag precursor. As such, while the nucleocapsid (NC) domain specifically recruits two copies of the FL-RNA, the matrix (MA) domain allows targeting of the complex to specific plasma membrane micro-domains and the capsid (CA) domain drives Gag multimerization at such sites. Packaging of two copies of the FL-RNA by the NC domain of Gag is highly specific and occurs selectively over thousands of cellular and viral RNA species. This selectivity was proposed to be possible by the presence of *cis*-acting RNA signatures spanning the 5′-UTR and the beginning of the Gag coding region (51). However, the FL-RNA also serves as mRNA for the synthesis of Gag and Gag-Pol precursors and recent work using single molecule FISH coupled to the SunTag system showed that a FL-RNA molecule accomplishes one of these functions at a time (7). Recent data also suggest that the adoption of a dimerization prone conformation could be determined by the selection of the transcription start site and the number of guanosine residues present at the very 5′ end of the FL-RNA (41–43). However, the precise mechanism(s) by which Gag distinguish and selects these 'packageable' FL-RNA molecules still remains elusive.

In this work, we propose that the presence of methylated adenosine residues in the form of m^{6}A interferes with packaging of the HIV-1 FL-RNA. Interestingly, we observed that a fraction of the Gag precursor is present in the nucleus and associates with the RNA demethylase FTO to promote demethylation of the FL-RNA, suggesting that Gag may contribute to FTO-mediated demethylation of those RNA molecules that will be used as genomic RNA to be incorporated into assembling viral particles (Figure 6). This idea is further reinforced by a recent study showing that Gag interacts with the FL-RNA at the transcription site (49) and suggest that FL-RNA molecules to be used for packaging are demethylated co-transcriptionally. This differential epitranscriptomic regulation exerted on the FL-RNA depending on its functions (mRNA or gRNA) may also help to explain the controversies reported in the literature (52). As such, while the presence of m^{6}A favors Gag synthesis through YTHDF proteins acting on the FL-RNA molecules destined to serve as mRNA (24), the same cytoplasmic m^{6}A readers may recognize specific features and drive degradation of the incoming viral RNA early upon infection (i.e. when the FL-RNA acts as gRNA) (25). Further studies are required to elucidate the mechanism by which the binding of YTHDF proteins to m^{6}A residues negatively impact FL-RNA metabolism in the absence of translation and whether methylation of the 5′-UTR is involved. In addition, the molecular mechanism by which the presence of m^{6}A at the 5′-UTR interferes with FL-RNA packaging also deserves further investigation.

Our experiments using the $\Delta A_{198}/\Delta A_{242}$ provirus suggest that these two adenosine residues together play a major role in the regulation of Gag synthesis and FL-RNA packaging. While A_{198} is located within the region complementary to the tRNA^{Lys3} at the primer binding site (PBS), A_{242} is located in the AGGA bulge at the base of the SL1 region and corresponds to a Gag-binding domain previously shown by chemical probing *in vitro* and *in virio* as well as by CLIP-seq studies (18,53,54). Although we showed the functional relevance of these two residues for the m^{6}A-mediated regulation of Gag synthesis and FL-RNA packaging, further studies are required to fully understand the precise mechanism by which these two adenosines impact FL-RNA metabolism. However, we showed that m^{6}A levels in the FL-RNA increase in the absence of adenosine 198 and 242 suggesting that these two residues are important in the regulation of m^{6}A methylation/demethylation of the viral transcript. Of note, increased m^{6}A levels in the FL-RNA

Downloaded from https://academic.oup.com/nar/article/50/4/2302/6524254 by guest on 11 April 2024

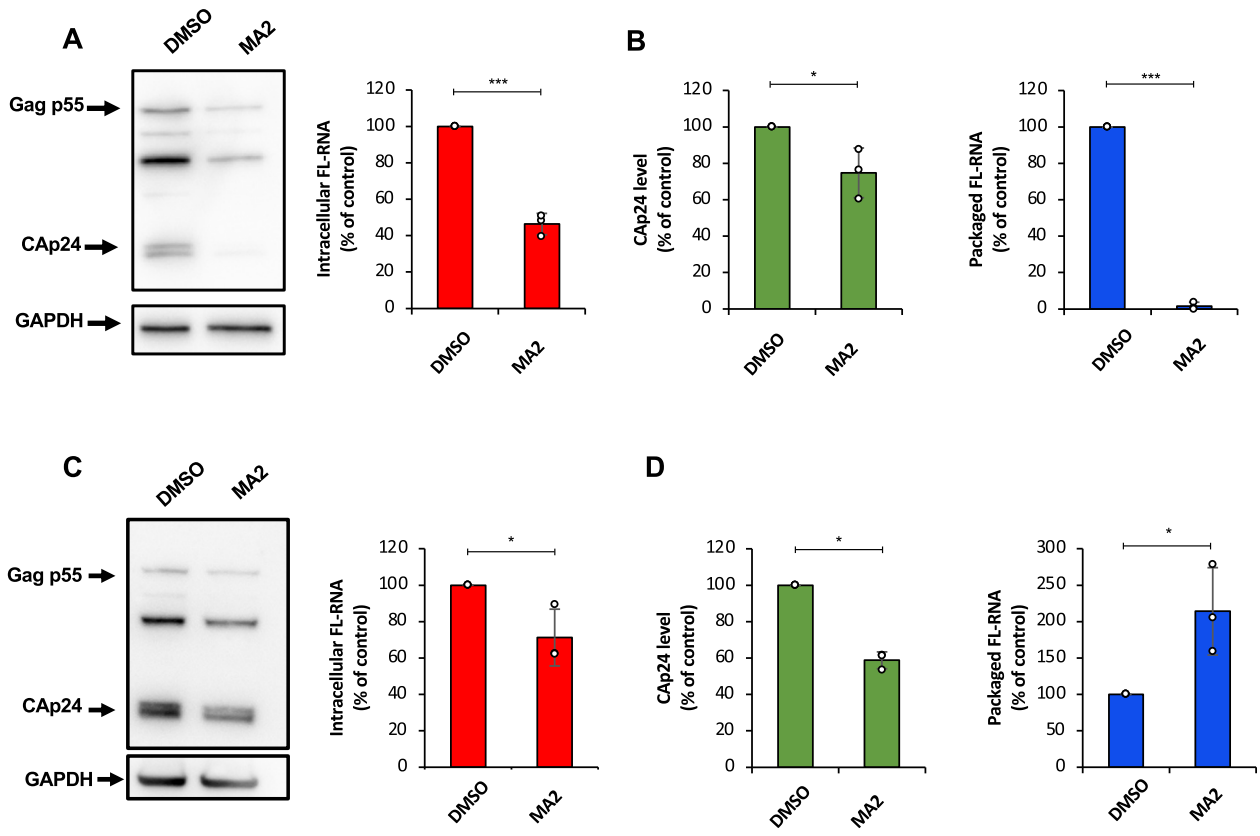

Figure 5. Inhibition of FTO demethylase activity impacts full-length RNA metabolism and blocks packaging. (**A**) HEK293T cells were transfected with pNL4.3 and pCMV-VSVg and were treated with MA2 or DMSO as a control. At 24 hpt, cells extracts were used to detect Gag and GAPDH as a loading control (left panel). In parallel, cells extracts were used to perform RNA extraction and the full-length RNA was quantified by RT-qPCR (right panel). The intracellular full-length RNA was normalized to the control (arbitrary set to 100%) and presented as the mean ± SD of three independent experiments (***$P < 0{,}001$, *t*-test). (**B**) Supernatants from (A) were filtered, and viral particles were concentrated by ultracentrifugation. The level of CAp24 was quantified by an anti-CAp24 ELISA, normalized to the control (arbitrary set to 100%) and presented as the mean ± SD of three independent experiments (ns; non-significant, *t*-test) (left panel). Purified viral particles were used to perform an RNA extraction and the packaged full-length RNA from CAp24 equivalents was quantified by RT-qPCR. Packaged full-length RNA was normalized to the control (arbitrary set to 100%) and presented as the mean +/− SD of three independent experiments (right panel). (**C**) and (**D**) The same experiment was performed using pNL4.3 $\Delta A_{198}/\Delta A_{242}$ (*$P < 0.05$, *t*-test).

of the double mutant virus resulted in increased Gag levels and reduced FL-RNA packaging in a way reminiscent to that observed under METTL3/14 overexpression using the wild type provirus thus, providing further evidence for the opposite impact of m^6A in defining the cytoplasmic fate of the FL-RNA. Since adenosine 198 and 242 reside in a Gag binding domain and our data showed that a Gag-FTO complex is important for FL-RNA demethylation, it is tempting to speculate that A_{198} and A_{242} participate in the recruitment of Gag-FTO onto the 5′-UTR to drive the demethylation of m^6A residues that is required for FL-RNA packaging. In addition to A_{198} and A_{242}, residues A_{16}, A_{47}, A_{55} in the TAR motif, A_{124}, A_{133}, A_{149}, A_{192} in the PBS structure and A_{311} around the packaging signal within the 5′-UTR of the NL4.3 FL-RNA are also in the DRACH context and, therefore could be interfering with packaging when methylated.

In contrast to the simple retrovirus MLV, which segregates its FL-RNA into two separate populations for translation and packaging, the FL-RNA of the human lentivirus HIV-1 was proposed to exist as a single population that can indistinctly serve as mRNA or gRNA. Recent work showed that the cytoplasmic fate of the MLV FL-RNA is specified by the export pathway employed to exit the nucleus. As such, MLV FL-RNA molecules exported through the Tap/NXF1 or CRM1 pathways were used for Gag synthesis or packaging, respectively (55). Such a specification is unlikely to occur during HIV-1 replication since Rev/CRM1-dependent nuclear export has been shown to be critical for efficient Gag synthesis and FL-RNA packaging (56,57). However, the recent report from Chen and colleagues (7) demonstrated that despite the FL-RNA present in the cytoplasm is able to accomplish both functions, only half of the cytoplasmic FL-RNA is actively translated. Moreover, the authors also presented evidence showing that Gag only associates with non-translating RNA further suggesting that co-translational packaging is not a major driver of FL-RNA selection by Gag. Authors also reported that FL-RNA molecules that have been translated do not associate with Gag even when they are no longer translating, supporting the existence of two populations specialized to accomplish functions as mRNA or gRNA. These data support our

Downloaded from https://academic.oup.com/nar/article/50/4/2302/6524254 by guest on 11 April 2024

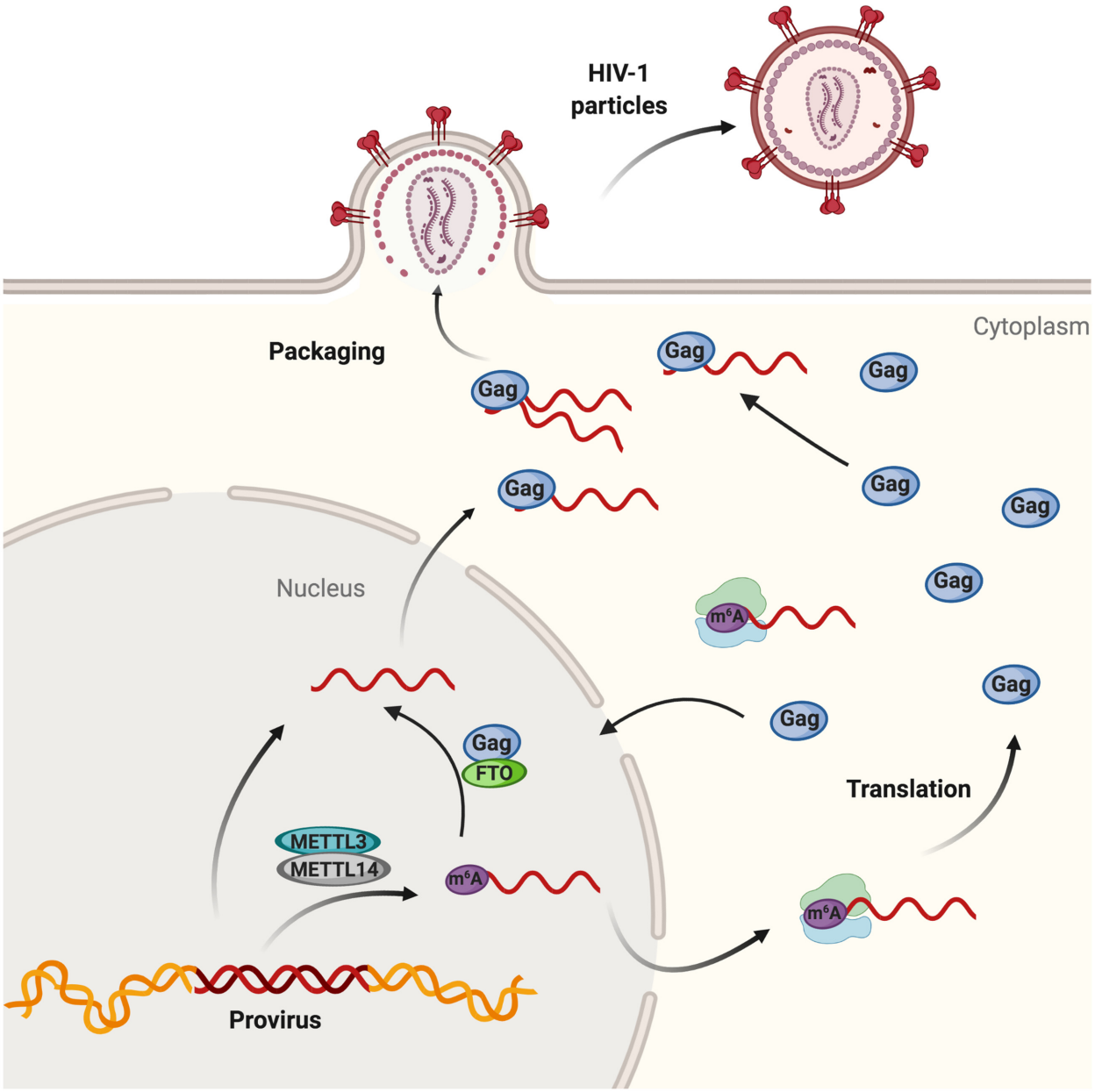

Figure 6. Working model for the epitranscriptomic regulation of HIV-1 full-length RNA packaging. The HIV-1 full-length RNA is methylated by the METTL3/14 complex in the nucleus (for simplicity, only the presence of m^{6}A on the 5′-UTR is shown). A fraction of the structural protein Gag is imported to the nucleus, interacts with the m^{6}A eraser FTO to promote demethylation of adenosines residues present at the 5′-UTR in a process required for full-length RNA packaging (created with BioRender).

idea that the HIV-1 FL-RNA may exist as two populations with different m^{6}A patterns. From these two populations, those molecules lacking m^{6}A at the 5′-UTR will be preferentially selected by Gag for packaging (Figure 6).

Since HIV-1 FL-RNA dimerization and packaging are two tightly connected processes, the relationship between m^{6}A and dimerization deserves further investigation. Studies carried out in living cells have demonstrated that HIV-1 FL-RNA dimerization is promoted by Gag and occurs at the plasma membrane (9,11). This contrasts to MLV FL-RNA dimerization, which was shown to occur at the transcription site (58,59). Considering that HIV-1 FL-RNA dimerization has been shown to depend on the adoption of a three-way junction structure adopted based on the selection of the transcription site (15), it would be of interest to investigate whether m^{6}A residues within the 5′-UTR impact on the adoption of a dimerization prone structure and/or in the dimerization process *per se*. Indeed, previous studies have shown that the presence of m^{6}A can alter RNA folding (60). However, it is also possible that the presence of m^{6}A influence 5′-UTR folding indirectly through the recruitment of m^{6}A readers. Alternatively, the presence of m^{6}A within the 5′-UTR could interfere with packaging by impeding Gag recruitment either directly by repealing

Downloaded from https://academic.oup.com/nar/article/50/4/2302/6524254 by guest on 11 April 2024

Gag binding (i.e. Gag is unable to bind an m^6A-containing binding site) or indirectly through steric hindrance imposed by m^6A readers. In this regard, studies carried out during HCV replication showed that the core protein binds preferentially to genomic RNA molecules lacking m^6A (61).

Although the reversibility of adenosine methylation as well as the main target of the RNA demethylase FTO have been recently challenged (45,62), we showed that the HIV-1 FL-RNA is a substrate for FTO and this RNA demethylase is able to regulate the incorporation of the viral genome into released viral particles. Interestingly, treatment of HIV-1 producer cells with the specific FTO inhibitor meclofenamic acid resulted in an impairment of FL-RNA metabolism with a potent effect on packaging, confirming the critical role of the demethylase activity of FTO during viral replication. In addition to meclofenamic acid, two small molecules developed by structure-based rational design were recently described as specific inhibitors of the FTO m^6A demethylase activity with the potential to be used as a treatment for adult myeloid leukemia (63). Therefore, this novel epitranscriptomic mechanism regulating packaging of the HIV-1 FL-RNA could also be exploited as a target for pharmacological intervention.

DATA AVAILABILITY

MeRIP-seq data were deposited at the GEO of the NCBI (accession number Nº GSE130687).

SUPPLEMENTARY DATA

Supplementary Data are available at NAR Online.

ACKNOWLEDGEMENTS

Authors wish to thank Professor Cai-Guang Yang (CAS Key Laboratory of Receptor Research, Shangai Institute of Materia Medica, Chinese Academy of Sciences) for providing MA2. Authors will also thank to Dr. Chuan He (University of Chicago) and Dr. Yun-Gui Yang (Beijing Institute of Genomics, Chinese Academy of Sciences) for providing different plasmids used in this study.

Author contributions: C.P.M. designed and performed experiments, analyzed data and wrote the paper. D.T.A., A.G.A., S.R.B., B.R.A., F.G.deG., P.A.C., C.A.S., M.L.A. and J.Ch. performed experiments and analyzed data. C.R.F. performed bioinformatic analyses. F.V.E. contributed to data analysis and manuscript writing. R.S.R. contributed to the concept and design of the study, data analysis, manuscript writing and funding acquisition. All the authors read and approved the final version of the manuscript.

FUNDING

FONDECYT Program [1160176, 1190156 to R.S.R., 1180798, 1211547 to F.V.E., 11180621 to D.T.A.]; ANID - ICM [ICN2021_045 to R.S.-R.]; C.P.M., C.A.S., A.G.A., F.G.deG., S.R.B., B.R.A. and P.A.C. are recipients of a National Doctoral fellowship from CONICYT. Funding for open access charge: FONDECYT [1190156].

Conflict of interest statement. None declared.

REFERENCES

1. Karn,J. and Stoltzfus,C.M. (2012) Transcriptional and posttranscriptional regulation of HIV-1 gene expression. *Cold Spring Harb. Perspect. Med.*, **2**, a006916.
2. Butsch,M. and Boris-lawrie,K. (2002) Destiny of unspliced retroviral RNA: ribosome and/or virion? *J. Virol.*, **76**, 3089–3094.
3. Mailler,E., Bernacchi,S., Marquet,R., Paillart,J.C., Vivet-Boudou,V. and Smyth,R.P. (2016) The life-cycle of the HIV-1 gag–RNA complex. *Viruses*, **8**, 248.
4. Levin,J.G., Grimley,P.M., Ramseur,J.M. and Berezesky,I.K. (1974) Deficiency of 60 to 70S RNA in murine leukemia virus particles assembled in cells treated with actinomycin D. *J. Virol.*, **14**, 152–161.
5. Levin,J.G. and Rosenak,M.J. (1976) Synthesis of murine leukemia virus proteins associated with virions assembled in actinomycin d treated cells: evidence for persistence of viral messenger RNA. *Proc. Natl. Acad. Sci. U.S.A.*, **73**, 1154–1158.
6. Dorman,N. and Lever,A. (2000) Comparison of viral genomic RNA sorting mechanisms in human immunodeficiency virus type 1 (HIV-1), HIV-2, and moloney murine leukemia virus. *J. Virol.*, **74**, 11413–11417.
7. Chen,J., Liu,Y., Wu,B., Nikolaitchik,O.A., Mohan,P.R., Chen,J., Pathak,V.K. and Hu,W.S. (2020) Visualizing the translation and packaging of HIV-1 full-length RNA. *Proc. Natl. Acad. Sci. U.S.A.*, **117**, 6154–6155.
8. Laughrea,M., Jetté,L., Mak,J., Kleiman,L., Liang,C. and Wainberg,M.A. (1997) Mutations in the kissing-loop hairpin of human immunodeficiency virus type 1 reduce viral infectivity as well as genomic RNA packaging and dimerization. *J. Virol.*, **71**, 3397–3406.
9. Chen,J., Rahman,S.A., Nikolaitchik,O.A., Grunwald,D., Sardo,L., Burdick,R.C., Plisov,S., Liang,E., Tai,S., Pathak,V.K. *et al.* (2016) HIV-1 RNA genome dimerizes on the plasma membrane in the presence of gag protein. *Proc. Natl. Acad. Sci. U.S.A.*, **113**, E201–E208.
10. Clever,J.L. and Parslow,T.G. (1997) Mutant human immunodeficiency virus type 1 genomes with defects in RNA dimerization or encapsidation. *J. Virol.*, **71**, 3407–3414.
11. Ferrer,M., Clerté,C., Chamontin,C., Basyuk,E., Lainé,S., Hottin,J., Bertrand,E., Margeat,E. and Mougel,M. (2016) Imaging HIV-1 RNA dimerization in cells by multicolor super-resolution and fluctuation microscopies. *Nucleic Acids Res.*, **44**, 7922–7934
12. Huthoff,H. and Berkhout,B. (2001) Two alternating structures of the HIV-1 leader RNA. *RNA*, **7**, 143–157.
13. Berkhout,B., Ooms,M., Beerens,N., Huthoff,H., Southern,E. and Verhoef,K. (2002) In vitro evidence that the untranslated leader of the HIV-1 genome is an RNA checkpoint that regulates multiple functions through conformational changes. *J. Biol. Chem.*, **277**, 19967–19975.
14. Abbink,T.E.M. and Berkhout,B. (2003) A novel long distance base-pairing interaction in human immunodeficiency virus type 1 rna occludes the gag start codon. *J. Biol. Chem.*, **278**, 11601–11611.
15. Keane,S.C., Heng,X., Lu,K., Kharytonchyk,S., Ramakrishnan,V., Carter,G., Barton,S., Hosic,A., Florwick,A., Santos,J. *et al.* (2015) Structure of the HIV-1 RNA packaging signal. *Science*, **348**, 917–921.
16. Kuzembayeva,M., Dilley,K., Sardo,L. and Hu,W.S. (2014) Life of psi: how full-length HIV-1 RNAs become packaged genomes in the viral particles. *Virology*, **454–455**, 362–370.
17. Watts,J.M., Dang,K.K., Gorelick,R.J., Leonard,C.W., Bess,J.W., Swanstrom,R., Burch,C.L. and Weeks,K.M. (2009) Architecture and secondary structure of an entire HIV-1 RNA genome. *Nature*, **460**, 711–716.
18. El-Wahab,E.W.A., Smyth,R.P., Mailler,E., Bernacchi,S., Vivet-Boudou,V., Hijnen,M., Jossinet,F., Mak,J., Paillart,J.C. and Marquet,R. (2014) Specific recognition of the HIV-1 genomic RNA by the gag precursor. *Nat. Commun.*, **5**, 4304.
19. Siegfried,N.A., Busan,S., Rice,G.M., Nelson,J.A.E. and Weeks,K.M. (2014) RNA motif discovery by SHAPE and mutational profiling (SHAPE-MaP). *Nat. Methods*, **11**, 959–965.
20. Paillart,J.C., Dettenhofer,M., Yu,X.F., Ehresmann,C., Ehresmann,B. and Marquet,R. (2004) First snapshots of the HIV-1 RNA structure in infected cells and in virions. *J. Biol. Chem.*, **279**, 48397–48403.
21. Abbink,T.E.M., Ooms,M., Haasnoot,P.C.J. and Berkhout,B. (2005) The HIV-1 leader RNA conformational switch regulates RNA

Downloaded from https://academic.oup.com/nar/article/50/4/2302/6524254 by guest on 11 April 2024

dimerization but does not regulate mRNA translation. *Biochemistry*, **44**, 9058–9066.
22. Boeras,I., Seufzer,B., Brady,S., Rendahl,A., Heng,X. and Boris-Lawrie,K. (2017) The basal translation rate of authentic HIV-1 RNA is regulated by 5′UTR nt-pairings at junction of r and u5. *Sci. Rep.*, **7**, 6902.
23. Lichinchi,G., Gao,S., Saletore,Y., Gonzalez,G.M., Bansal,V., Wang,Y., Mason,C.E. and Rana,T.M. (2016) Dynamics of the human and viral m 6 a RNA methylomes during HIV-1 infection of t cells. *Nat. Microbiol.*, **1**, 16011.
24. Kennedy,E.M., Bogerd,H.P., Kornepati,A.V.R., Kang,D., Ghoshal,D., Marshall,J.B., Poling,B.C., Tsai,K., Gokhale,N.S., Horner,S.M. *et al.* (2016) Posttranscriptional m6A editing of HIV-1 mRNAs enhances viral gene expression. *Cell Host Microbe*, **19**, 675–685.
25. Tirumuru,N., Zhao,B.S., Lu,W. and Lu,Z. (2016) N6 -methyladenosine of HIV-1 RNA regulates viral infection and HIV-1 gag protein expression. *elife*, **5**, e15528.
26. Lu,W., Tirumuru,N., Gelais,C.S., Koneru,P.C., Liu,C., Kvaratskhelia,M., He,C. and Wu,L. (2018) N6-Methyladenosine–binding proteins suppress HIV-1 infectivity and viral production. *J. Biol. Chem.*, **293**, 12992–13005.
27. Toro-Ascuy,D., Rojas-Araya,B., García-de-Gracia,F., Rojas-Fuentes,C., Pereira-Montecinos,C., Gaete-Argel,A., Valiente-Echeverría,F., Ohlmann,T. and Soto-Rifo,R. (2018) A Rev–CBP80–eIF4AI complex drives gag synthesis from the HIV-1 unspliced mRNA. *Nucleic Acids Res.*, **46**, 11539–11552.
28. Mangeot,P.-E., Nègre,D., Dubois,B., Winter,A.J., Leissner,P., Mehtali,M., Kaiserlian,D., Cosset,F.-L. and Darlix,J.-L. (2000) Development of minimal lentivirus vectors derived from simian immunodeficiency virus (SIVmac251) and their use for gene transfer into human dendritic cells. *J. Virol.*, **74**, 8307–8315.
29. Liu,J., Yue,Y., Han,D., Wang,X., Fu,Y., Zhang,L., Jia,G., Yu,M., Lu,Z., Deng,X. *et al.* (2014) A METTL3-METTL14 complex mediates mammalian nuclear RNA N6-adenosine methylation. *Nat. Chem. Biol.*, **10**, 93–95.
30. Zheng,G., Dahl,J.A., Niu,Y., Fedorcsak,P., Huang,C.M., Li,C.J., Vågbø,C.B., Shi,Y., Wang,W.L., Song,S.H. *et al.* (2013) ALKBH5 is a mammalian RNA demethylase that impacts RNA metabolism and mouse fertility. *Mol. Cell*, **49**, 18–29.
31. Jia,G., Fu,Y., Zhao,X., Dai,Q., Zheng,G., Yang,Y., Yi,C., Lindahl,T., Pan,T., Yang,Y. *et al.* (2011) N 6-Methyladenosine in nuclear RNA is a major substrate of the obesity-associated FTO. *Nat. Chem. Biol.*, **7**, 6–9.
32. Soto-Rifo,R., Rubilar,P.S. and Ohlmann,T. (2013) The DEAD-box helicase DDX3 substitutes for the cap-binding protein eIF4E to promote compartmentalized translation initiation of the HIV-1 genomic RNA. *Nucleic Acids Res.*, **41**, 6286–6299.
33. Schwartz,S., Felber,B.K. and Pavlakis,G.N. (1992) Distinct RNA sequences in the gag region of human immunodeficiency virus type 1 decrease RNA stability and inhibit expression in the absence of rev protein. *J. Virol.*, **66**, 150–159.
34. Fröhlich,A., Rojas-Araya,B., Pereira-Montecinos,C., Dellarossa,A., Toro-Ascuy,D., Prades-Pérez,Y., García-de-Gracia,F., Garcés-Alday,A., Rubilar,P.S., Valiente-Echeverría,F. *et al.* (2016) DEAD-box RNA helicase DDX3 connects CRM1-dependent nuclear export and translation of the HIV-1 unspliced mRNA through its N-terminal domain. *Biochim. Biophys. Acta - Gene Regul. Mech.*, **1859**, 719–730.
35. Feng,J., Liu,T. and Zhang,Y. (2011) Using MACS to identify peaks from chip-seq data. *Curr. Protoc. Bioinformatics*, **Chapter 2**, Unit 2.14.
36. Zhou,Y., Zeng,P., Li,Y.H., Zhang,Z. and Cui,Q. (2016) SRAMP: prediction of mammalian N6-methyladenosine (m6A) sites based on sequence-derived features. *Nucleic Acids Res.*, **44**, e91.
37. García-de-Gracia,F., Gaete-Argel,A., Riquelme-Barrios,S., Pereira-Montecinos,C., Rojas-Araya,B., Aguilera,Paulina, Oyarzún-Arrau,A., Rojas-Fuentes,C., Acevedo,M.L, Chnaiderman,J., Valiente-Echeverría,F., Toro-Ascuy,D. and Soto-Rifo,R. (2021) CBP80/20-dependent translation initiation factor (CTIF) inhibits HIV-1 Gag synthesis by targeting the function of the viral protein Rev. *RNA Biol.*, **18**, 745–758.
38. Briggs,J.A.G., Simon,M.N., Gross,I., Kräusslich,H.G., Fuller,S.D., Vogt,V.M. and Johnson,M.C. (2004) The stoichiometry of gag protein in HIV-1. *Nat. Struct. Mol. Biol.*, **11**, 672–675.
39. Onafuwa-Nuga,A.A., Telesnitsky,A. and King,S.R. (2006) 7SL RNA, but not the 54-kd signal recognition particle protein, is an abundant component of both infectious HIV-1 and minimal virus-like particles. *RNA*, **12**, 542–546.
40. Houzet,L., Paillart,J.C., Smagulova,F., Maurel,S., Morichaud,Z., Marquet,R. and Mougel,M. (2007) HIV controls the selective packaging of genomic, spliced viral and cellular RNAs into virions through different mechanisms. *Nucleic Acids Res.*, **35**, 2695–2704.
41. Kharytonchyk,S., Monti,S., Smaldino,P.J., Van,V., Bolden,N.C., Brown,J.D., Russo,E., Swanson,C., Shuey,A., Telesnitsky,A. *et al.* (2016) Transcriptional start site heterogeneity modulates the structure and function of the HIV-1 genome. *Proc. Natl. Acad. Sci. U.S.A.*, **113**, 13378–13383.
42. Masuda,T., Sato,Y., Huang,Y.L., Koi,S., Takahata,T., Hasegawa,A., Kawai,G. and Kannagi,M. (2015) Fate of HIV-1 cDNA intermediates during reverse transcription is dictated by transcription initiation site of virus genomic RNA. *Sci. Rep.*, **5**, 17680.
43. Brown,J.D., Kharytonchyk,S., Chaudry,I., Iyer,A.S., Carter,H., Becker,G., Desai,Y., Glang,L., Choi,S.H., Singh,K. *et al.* (2020) Structural basis for transcriptional start site control of HIV-1 RNA fate. *Science*, **368**, 413–417.
44. Keane,S.C., Van,V., Frank,H.M., Sciandra,C.A., McCowin,S., Santos,J., Heng,X. and Summers,M.F. (2016) NMR detection of intermolecular interaction sites in the dimeric 5′-leader of the HIV-1 genome. *Proc. Natl. Acad. Sci. U.S.A.*, **113**, 13033–13038.
45. Darnell,R.R., Shengdong,K.E. and Darnell,J.E. (2018) Pre-mRNA processing includes N6 methylation of adenosine residues that are retained in mRNA exons and the fallacy of "RNA epigenetics". *RNA*, **24**, 262–267.
46. Lochmann,T.L., Bann,D. V., Ryan,E.P., Beyer,A.R., Mao,A., Cochrane,A. and Parent,L.J. (2013) NC-mediated nucleolar localization of retroviral gag proteins. *Virus Res.*, **171**, 304–318.
47. Maldonado,R.J.K., Rice,B., Chen,E.C., Tuffy,K.M., Chiari,E.F., Fahrbach,K.M., Hope,T.J. and Parent,L.J. (2020) Visualizing association of the retroviral gag protein with unspliced viral RNA in the nucleus. *MBio*, **11**, e00524-20.
48. Yu,K.L., Lee,S.H., Lee,E.S. and You,J.C. (2016) HIV-1 nucleocapsid protein localizes efficiently to the nucleus and nucleolus. *Virology*, **492**, 204–212.
49. Tuffy,K.M., Maldonado,R.J.K., Chang,J., Rosenfeld,P., Cochrane,A. and Parent,L.J. (2020) HIV-1 gag forms ribonucleoprotein complexes with unspliced viral RNA at transcription sites. *Viruses*, **12**, 1281.
50. Huang,Y., Yan,J., Li,Q., Li,J., Gong,S., Zhou,H., Gan,J., Jiang,H., Jia,G.F., Luo,C. *et al.* (2015) Meclofenamic acid selectively inhibits FTO demethylation of m6A over ALKBH5. *Nucleic Acids Res.*, **43**, 373–384.
51. Didierlaurent,L., Racine,P.J., Houzet,L., Chamontin,C., Berkhout,B. and Mougel,M. (2011) Role of HIV-1 RNA and protein determinants for the selective packaging of spliced and unspliced viral RNA and host U6 and 7SL RNA in virus particles. *Nucleic Acids Res.*, **39**, 8915–8927.
52. Riquelme-Barrios,S., Pereira-Montecinos,C., Valiente-Echeverría,F. and Soto-Rifo,R. (2018) Emerging roles of N^6-methyladenosine on HIV-1 RNA metabolism and viral replication. *Front. Microbiol.*, **9**, 576.
53. Kutluay,S.B., Zang,T., Blanco-Melo,D., Powell,C., Jannain,D., Errando,M. and Bieniasz,P.D. (2014) Global changes in the RNA binding specificity of HIV-1 gag regulate virion genesis. *Cell*, **159**, 1096–1109.
54. Wilkinson,K.A., Gorelick,R.J., Vasa,S.M., Guex,N., Rein,A., Mathews,D.H., Giddings,M.C. and Weeks,K.M. (2008) High-throughput SHAPE analysis reveals structures in HIV-1 genomic RNA strongly conserved across distinct biological states. *PLoS Biol.*, **6**, 883–899.
55. Mougel,M., Akkawi,C., Chamontin,C., Feuillard,J., Pessel-Vivares,L., Socol,M. and Laine,S. (2020) NXF1 and CRM1 nuclear export pathways orchestrate nuclear export, translation and packaging of murine leukaemia retrovirus unspliced RNA. *RNA Biol.*, **4**, 528–538.
56. Toro-Ascuy,D., Rojas-Araya,B., García-de-Gracia,F., Rojas-Fuentes,C., Pereira-Montecinos,C., Gaete-Argel,A.,

Downloaded from https://academic.oup.com/nar/article/50/4/2302/6524254 by guest on 11 April 2024

Valiente-Echeverría,F., Ohlmann,T. and Soto-Rifo,R. (2018) A Rev–CBP80–eIF4AI complex drives gag synthesis from the HIV-1 unspliced mRNA. *Nucleic Acids Res.*, **46**, 11539–11552.
57. Blissenbach,M., Grewe,B., Hoffmann,B., Brandt,S. and Überla,K. (2010) Nuclear RNA export and packaging functions of HIV-1 rev revisited. *J. Virol.*, **84**, 6598–6604.
58. Flynn,J.A. and Telesnitsky,A. (2006) Two distinct moloney murine leukemia virus RNAs produced from a single locus dimerize at random. *Virology*, **344**, 391–400.
59. Maurel,S. and Mougel,M. (2010) Murine leukemia virus RNA dimerization is coupled to transcription and splicing processes. *Retrovirology*, **7**, 64.
60. Liu,N., Zhou,K.I., Parisien,M., Dai,Q., Diatchenko,L. and Pan,T. (2017) N6-methyladenosine alters RNA structure to regulate binding of a low-complexity protein. *Nucleic Acids Res.*, **45**, 6051–6063.
61. Gokhale,N.S., McIntyre,A.B.R., McFadden,M.J., Roder,A.E., Kennedy,E.M., Gandara,J.A., Hopcraft,S.E., Quicke,K.M., Vazquez,C., Willer,J. *et al.* (2016) N6-Methyladenosine in flaviviridae viral RNA genomes regulates infection. *Cell Host Microbe*, **20**, 654–665.
62. Mauer,J. and Jaffrey,S.R. (2018) FTO, m 6 a m, and the hypothesis of reversible epitranscriptomic mRNA modifications. *FEBS Lett.*, **592**, 2012–2022.
63. Huang,Y., Su,R., Sheng,Y., Dong,L., Dong,Z., Xu,H., Ni,T., Zhang,Z.S., Zhang,T., Li,C. *et al.* (2019) Small-Molecule targeting of oncogenic FTO demethylase in acute myeloid leukemia. *Cancer Cell*, **35**, 677–691.

Downloaded from https://academic.oup.com/nar/article/50/4/2302/6524254 by guest on 11 April 2024